interactIVe

Accident avoidance by active intervention for Intelligent Vehicles

Deliverable D5.1 | Vehicle Dynamics Model & Path Stability Control Algorithms

Version	2.1
Dissemination	PU
Project Coordination	FFA
Due Date	2013-02-18
Version Date	2013-02-20

7th Framework Programme
ICT-2009.6.1: ICT
for Safety and Energy Efficiency in Mobility
Grant Agreement No. 246587
Large-scale Integrated Project
www.interactIVe-ip.eu

SEVENTH FRAMEWORK PROGRAMME

Authors

Arman Nozad – CHAL
Morteza Hassanzadeh – CHAL
Mathias Lidberg – CHAL
Jitendra Shah – FFA

Project Coordinator

Aria Etemad
Ford Research & Advanced Engineering Europe

Suesterfeldstr. 200
52072 Aachen
Germany

Phone: +49 241 9421 246
Fax: +49 241 9421 301
Email: aetemad1@ford.com

Version control

Version	Date	Description
0.1	2011-07-01	First draft version by CHAL.
0.2	2011-07-07	Peer review version by CHAL.
0.3	2011-07-08	Peer review version by CHAL including FFA material.
0.4	2011-07-18	Peer review feedback from FFA and VTEC included.
0.5	2011-08-12	Reworked chapter 7-10 by CHAL.
1.0	2011-10-14	Reworked chapter 1-3, 5-8, 11, 12, finalised version by CHAL.
1.1	2012-12-07	Experimental verification of the model was updated using new test data. Tyre model modified to a simplified combined slip tyre model, and the documentation moved to a separate document. Discrete input information were added to the model, to include comments of the reviewers from review P2. Chapters 1, 2 , 4-9 were reworked.
1.2	2013-02-05	Controller was modified. All simulation results updated. A simple model of steering was added. Chapters 1, 2 , 4-9 were reworked.
1.3	2013-02-08	Tyre documentation was added as an appendix. Reworked Chapter 5.
1.4	2013-02-11	Deliverable structure was added to the introduction. Chapter 4 moved after first Chapter. Reworked chapters 1, 3, 5-9.
1.5	2013-02-18	Deliverable structure was modified and number of Chapters reduced from 12 to 8. Optimal control and control design were modified and simulation results were updated. Peer review feedback from VTEC included. Reworked Chapters 1-6 in the new structure.
2.0	2013-02-19	Finalized version by Chalmers. Comments of the reviewers from review P2 are further included, and new references made, also to previous EU projects. Chapter 1, 8 reworked
2.1	2013-02-20	Layout check performed by EICT.

Table of contents

Figures

Tables

1 Introduction

Traffic safety is a major requirement for transportation systems. A lot of work has been done in the passive safety area where milliseconds during a crash are of high importance. Nowadays, collision avoidance in the field of active safety is more prioritised. Accident avoidance by active intervention for Intelligent Vehicles is the headline of the large European project *interactIVe* [1]. interactIVe has the objective to develop new integrated Advanced Driver Assistance Systems (ADAS). Several subprojects are defined in this project, including *INCA* that aims for INtegrated Collision Avoidance by combining longitudinal and lateral control of the vehicle to prevent possible accidents.

As a contribution to INCA, this study focuses on autonomous path stability control of heavy vehicles and passenger cars, which may serve as a basis for active intervention, particularly intended for helping the driver in emergency collision avoidance manoeuvres.

1.1 Deliverable structure

Autonomous path stability control is a challenging control problem from several perspectives. Starting with the use cases of interest, the scope of the report and the delimitations of the study are included in Chapter 1. A review of related works closes the first chapter.

There are several possible actuator configurations available for longitudinal and lateral control. Therefore a methodology based on optimal control is used in Chapter 2 to investigate the potential of various actuator configurations to perform a manoeuvre.

Proper vehicle dynamics models that can capture the important aspects of the controlled vehicles dynamics, are essential for simulations. For the heavy vehicle dynamics, a model with limited complexity is used in this work, as described in Chapter 3. The details of the used tyre model are appended to this deliverable as Appendix A. Heavy vehicles are considered throughout the report but for passenger cars simulation settings and results are presented in one place in Chapter 7. The corresponding controller is implemented in the passenger car demonstrator from FFA.

For the collision avoidance manoeuvres defined based on the use cases, a generic path planning procedure generates an appropriate 5th order polynomial reference path. Analytical calculations of the coefficients for the fifth order polynomial are appended to this deliverable as Appendix B. In order for the vehicle to follow the reference path, a path and speed control system is designed and used that provides the actuators with suitable feedforward and feedback inputs. Description and details of the path planning and control algorithms come in Chapter 4.

Using the heavy vehicle dynamics model and path and speed control system, all 3 use cases are simulated, and results are presented in Chapter 5.

Using rapid control prototyping, an early version of the control system was implemented on the heavy vehicle demonstrator from Volvo Truck. Some experiments were carried out at the test track and the measured data is used for both model verification and a preliminary evaluation of the controller performance, as presented in Chapter 6.

In summary, as one of the major aims of this work, a simulation environment is developed that can be used for further studies and investigation of both the heavy vehicle dynamics model and the path stability control algorithms. Suggested future work is included in Chapter 8.

1.2 Use cases

Key transportation problems that the interactIVe functions should address are described as *target scenarios*. Based on the target scenarios and user needs assessment, *use cases* are developed to define how the problems described in the target scenarios should be solved by interactIVe functions. Thus the use cases can serve as the basis for defining the *functional requirements*. In the interactIVe project, target scenarios and functional requirements are defined by the vertical subprojects including SP5, INCA.

Aiming for integrated collision avoidance, INCA is required to consider several target scenarios and functionalities [2]. In the flow of a target scenario, various use cases may be involved that can address functional requirements in an integrated collision avoidance application. Based on the sensor information, traffic situation is under continuous assessment while different functions are ready to act upon an upcoming event. If an imminent collision or undesirable road departure is detected, the appropriate reaction to the situation with respect to warning or intervention will be taken by the application. First the application warns the driver. If the driver did not react to the warning, the application intervenes and starts a suitable autonomous collision avoidance manoeuvre by utilising all capabilities including available actuators. While other works consider warning the driver or make sure that there is possibility on the road to perform a certain manoeuvre, *e.g.* if there is a free adjacent lane to do a lane change, the focus of this work is on the intervention by utilising the actuators. Therefore 3 use cases are considered in this work that can represent fundamental aspects of a generic intervention solution for integrated collision avoidance application. These use cases are introduced in this section, whereas complete description and details of all use cases and requirements can be found in Deliverable D1.5 [3].

Although this work includes both heavy vehicle and passenger car, emphasis of the work is on the heavy vehicle. Therefore, heavy vehicle is intended in the discussions and for the graphical representations unless specified for the passenger car, *e.g.* as in Chapter 7. By the host vehicle, HV, which is the vehicle that is equipped with the application fulfilling a function or the system addressed by the use case, the heavy vehicle is intended accordingly.

1.2.1 Rear-end collision avoidance (RECA)

The use case Rear-End Collision Avoidance, RECA, describes situations in which the host vehicle have a higher velocity than the vehicle in front, the lead vehicle, LV. The lead vehicle may be either moving slowly or stopped in front of the host vehicle. The speed of the host vehicle and relative speed of the vehicles may vary up to $100\ \mathrm{km/h}$ and $60\ \mathrm{km/h}$, respectively [3]. Figure 1.1 shows a schematic example of the use case. It is assumed that the lead vehicle is stopped in front of the host vehicle Figure 1.1.a, and if the collision avoidance application starts an intervention, pair of possible manoeuvres are shown in the figure. A braking manoeuvre, Figure 1.1.b, would stop the host vehicle by the end of the required longitudinal distance, d, or a steering manoeuvre, Figure 1.1.c, would perform a lane change with lateral displacement of b for the same required longitudinal distance to avoid the collision.

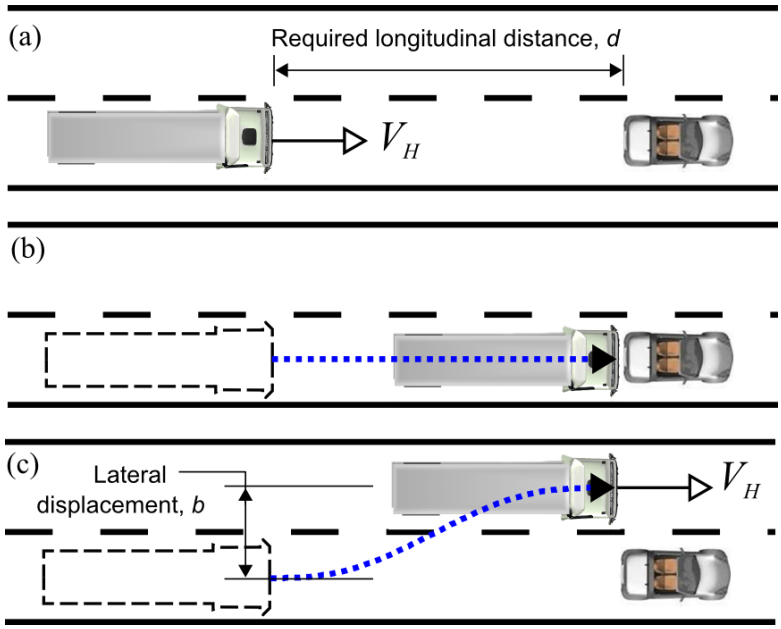

Figure 1.1 RECA manoeuvre (a) with a pair of possible actuator configurations; braking only (b), and single lane change (c).

1.2.2 Run-off road prevention (RORP) on a straight road

The use case Run-Off Road Prevention, RORP, on a straight road describes undesirable departure of the vehicle from the lane due to *e.g.* drowsiness of the driver. The speed of the host vehicle may range from 25 to 90 $\mathrm{km/h}$ [3]. Figure 1.2 shows a schematic sketch of the use case, and a possible steering manoeuvre that would return the vehicle back to the lane by a required longitudinal distance, d.

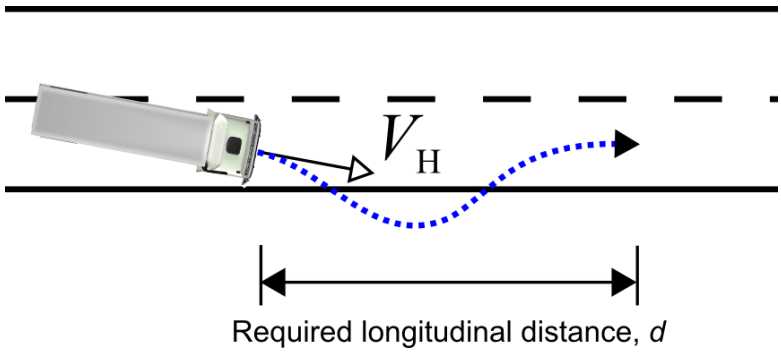

Figure 1.2 RORP on a straight road.

1.2.3 Run-off road prevention (RORP) in a curve

This use case deals with the vehicle driving on a curved road with a rather large radius. The lack of action from driver departs the truck from the road. The speed of the host vehicle may range from 38 to 85 $\mathrm{km/h}$ [3]. Figure 1.3 shows a schematic sketch of the use case, and a possible steering manoeuvre that would return the vehicle back to the lane by a required longitudinal distance, d.

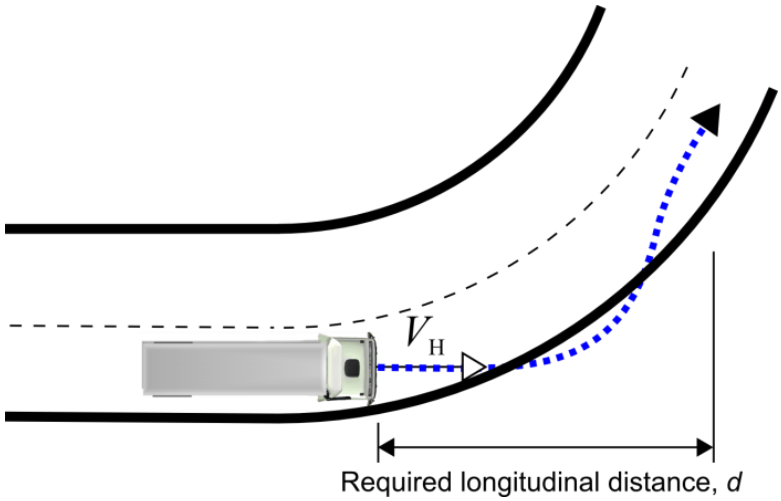

Figure 1.3 RORP in a curve.

1.3 Scope

The work documented in this report can be summarized as:

- Development of a flexible simulation environment for path stability control of passenger cars and heavy vehicles.
- Development of path controller aimed for integrated longitudinal and lateral control using integrated braking and steering.
- Simulation and analysis of the controller performance to determine important requirements on e.g. sensors and communication.

This scope is quite broad. To narrow it down particular focus is put on path stability control on the limits by:

- Determining the potential of using various actuator configurations using an optimal control methodology for a simplified vehicle model. The actuator configurations considered for this study are:
  - *Steering*
  - *Braking*
  - *Integrated Braking and Steering*
- Implement one path planning procedure suitable for all considered use cases. The interaction between the path planning procedure and the low level steering controller is simulated and analyzed.
- Development of an path stability control by steering algorithm. The limitations of the algorithm is simulated and analyzed with respect to update rate of ego-vehicle lateral displacement and lateral speed estimation. Thus discrete control with given update rate is considered to understand what performance can be expected in practice.

The performance measures for path stability control on the limits can be stated as:

- All wheels must remain in contact with the road to avoid rollover.
- The lateral deviation from the reference path at the point where the obstacle is located should be as small as possible. This is important in order not to collide with the obstacle provided the reference path is desirably designed for the vehicle to follow and avoid the obstacle.

- The maximum path deviation should be as small as possible. This is especially important, for instance, in order for the vehicle not to depart from the road while or after avoiding the obstacle in front.
- The yaw stability and comfort should be acceptable.
- The requirements on the steering actuator.

1.4 Delimitations

In a complete collision avoidance system, the information about the road and ongoing traffic is acquired by a perception system, that employs different sources of information, e.g. built in sensors and cameras, and fuses necessary information to different functions through a perception horizon interface [4]. It is not within the scope of this work to study the perception horizon, and it is not modelled in any detail in this work, instead it is assumed that the necessary information is provided by the perception horizon. In the same way detailed analyses of various path planning approaches and the requirements for the accuracy of ego-vehicle positioning are not considered. The vehicle implementation of the path stability controller is ongoing work. It is expected that the simulations and analyses needs to be updated during this work.

The driver interaction and in particular driver steering override is not considered in this report. However, the wish of the driver to take over the control of the vehicle in the middle of a steering system intervention is the topic other ongoing work in InteractIVe.

Other delimitations are:

1.4.1 Vehicle chassis and tyre model

Rotating wheels and thus wheel slip is not included in the simulation model for heavy trucks. Instead a tailored tire model with brake force as input is employed to facilitate integration of braking and steering without including a brake control system that can be included in more detailed simulations at a later stage or considered in the actual vehicle.

1.4.2 Actuators and control system dynamics

- The entire reference input is estimated at the intervention start point.
- Only high-μ environment is considered; simulations on a low-μ surface requires a different tyre model.
- Steering actuator delays and dynamics are just partly modelled.

Delays due to slack in brake system are ignored. Instead, brake system is assumed to be pre-charged so that the effect of slack in brake performance is minute.

1.5 Related works

Safety systems to assist drivers in hazardous situations have evolved a lot over the past few decades. Several systems can help drivers to avoid potentially dangerous situations. Vehicle stability control systems uses data from the vehicle internal sensors to compare a driver's current estimated intended vehicle motion with the vehicle's actual motion to detect when a driver has lost control of a vehicle. The stability control system automatically intervenes by applying the brakes to individual wheels and possibly active steering to provide stability. In other words, these systems are reactive; they must detect a problem before corrective action can be taken. Since its introduction, stability control systems have had a tremendous impact

on vehicle safety. Recently sensor technologies such as camera and radar have enabled driver assistance systems beyond the concepts of stability control. Autonomous braking and steering interventions can mitigate collisions and also maintain vehicles on the intended path [5], [6], [7], and [8].

In contrast to stability control systems driving assistance systems considers intended path rather than vehicle motion and share control with the driver. An approach for driving assistance systems based on artificial potential fields is introduced by Gerdes and Rossetter [9] to assist the driver with the lane keeping task. Brake and steer interventions are superimposed on the driver's input and both safety and drivability is achieved using such a system.

Resende [10] implemented real-time trajectory planning in a dynamic environment applied to highly automated driving using a 5th order polynomial. The method was implemented for the HAVEit European project and it is fast and gives realistic behaviour. Using a similar approach for trajectory planning, Petrov [11] developed a nonlinear adaptive control scheme for an automated overtaking manoeuvre. The only information used for feedback control was the current inter-vehicle position and orientation.

Hiraoka *et.al.* [12] propose a path-tracking controller for a four wheel steering (4WS) vehicle based on the sliding mode control theory. By decoupling the front- and rear-wheel steering, an advantage is made in controlling the vehicle thus achieving more stability and more precision in path-tracking in comparison with 2WS. There are more robustness in stability against system uncertainties and perturbations.

An adaptive linear optimal control is employed by Thommyppillai *et.al.* [13] to drive the car at certain limits of handling. The advantages of using gain-scheduled adaptive control over a fixed-control scheme are shown in simulations of a virtual driver-controlled car. Kritayakirana and Gerdes [14], [15], and [16] describe the development of a race path-controller using integrated braking and steering system designed to drive a vehicle autonomously to its limits on an uneven dirt surface. The controller is be divided into four important parts, a path description, friction estimation, steering controller and slip circle longitudinal controller. A clothoid path is used to construct the desired path. Pre-knowledge of friction distribution is obtained from a ramp steer is used. Knowing the curvature, the feedforward steering input can be calculated and the steering feedback based on lane-keeping adds the robustness to the controller. Knowing the curvature of the track the longitudinal feedforward controller calculates the amount of throttle and brake for a desired trajectory. Longitudinal feedback controller based on slip circle fulfils two purposes. First, it provides a longitudinal input that controls tyre slip and secondly the slip circle controller ensures that the tyres are operating at their limits. This approach can maximize the tyre forces while effectively controlling the tyre slip.

2 Collision avoidance optimal control

The integrated longitudinal and lateral vehicle control in collision avoidance manoeuvres for various vehicle actuator configurations is not a trivial control problem. In order to determine the potential of using various actuator configurations and to benchmark the collision avoidance path and speed controller system developed later, the optimal control of a simplified vehicle model is studied here in a similar way as described in [17]. Here the simplified vehicle model is a point mass (particle vehicle model).

2.1 Particle model

The particle vehicle model depicted in Figure 2.1 has two degrees of freedom in horizontal plane OXY.

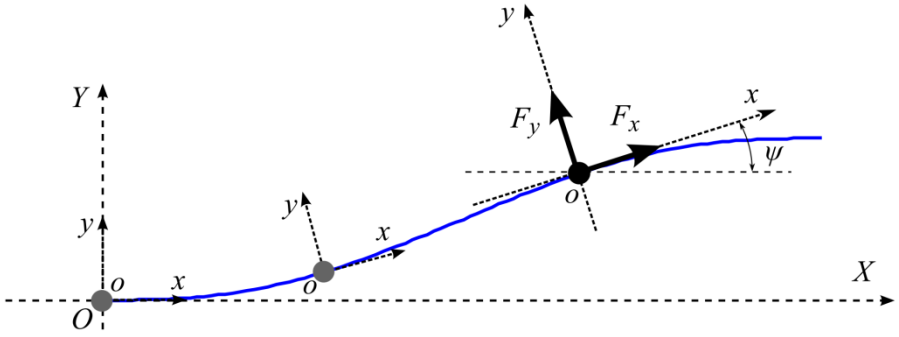

Figure 2.1 Schematic sketch of particle model in motion.

The total tyre forces commanded by the steering and braking actuators to control the vehicle motion is denoted F_y^D and F_x^D, respectively. The tyre force generation in not instantaneous in real tyres, therefore the tyre relaxation lengths (σ_x, σ_y) are taken into account to model the force generation delay. The actual forces from the tyres applied to the vehicle (F_x, F_y) are then determined by

$$\frac{\sigma_x}{v_x}\dot{F}_x + F_x = F_x^D, \tag{2.1}$$

$$\frac{\sigma_y}{v_x}\dot{F}_y + F_y = F_y^D. \tag{2.2}$$

The tyre forces are defined in a local coordinate system Oxy but the equations of motion are formulated in a global coordinate system OXY where the direction OX is the original track direction. The equations of planar motion for the vehicle particle model are:

$$\begin{aligned} m\ddot{X} &= F_x\cos\psi - F_y\sin\psi, \\ m\ddot{Y} &= F_x\sin\psi + F_y\cos\psi. \end{aligned} \tag{2.3}$$

In order to generate a particle model, which is capable of resembling the characteristics of a full vehicle model, a constraint considering the friction limit boundary on a "g-g" diagram and the rollover risk are added to the particle model. The total steering and braking forces are limited by a total tyre force ellipse (friction ellipse)

$$\left(\frac{a_x}{a_{x,\max}}\right)^2 + \left(\frac{a_y}{a_{y,\max}}\right)^2 \le 1 \tag{2.4}$$

where a_x and a_y are the longitudinal and lateral acceleration.

The considered set of collision avoidance manoeuvres for the use cases in Chapter 2 are defined by the initial and final conditions as given in Equations 2.5 and 2.6

$$V_x(0) = V_{x0}\,, \qquad V_y(0) = V_{y0}\,, \qquad X(0) = X_0\,, \qquad Y(0) = Y_0, \tag{2.5}$$

$$V_x(T) = V_{xT}\,, \qquad V_y(T) = V_{yT}\,, \qquad X(T) = X_T\,, \qquad Y(T) = Y_T, \tag{2.6}$$

where the parameters of the boundary conditions can be adjusted for each use case.

2.1 Optimal control

Introducing the state variables as $z = [X\ Y\ V_X\ V_Y\ F_x\ F_y]^T$, the planar equations of motion (Equations 2.1-2.3) can be transformed to a system of first order differential equations in the state space form.

$$\dot{z} = \begin{bmatrix} \dot{X} \\ \dot{Y} \\ \dot{V}_X \\ \dot{V}_Y \\ \dot{F}_x \\ \dot{F}_y \end{bmatrix} = \begin{bmatrix} V_x \\ V_y \\ (F_x \cos\psi - F_y \sin\psi)/m \\ (F_y \cos\psi + F_x \sin\psi)/m \\ (v_x/\sigma_x)(F_x^D - F_x) \\ (v_x/\sigma_y)(F_y^D - F_y) \end{bmatrix} \tag{2.7}$$

Then a general optimal control problem can be formulated in state space. The aim is to find states $z(t)$ and controls $u(t)$, which minimize the objective function

$$J(z,u) = c_0 z(0) + c_T z(T) + \int_0^T z^T Q z dt \tag{2.8}$$

subjected to the equations of motion from Equation 2.7

$$\dot{z}(t) = f(z,u), \tag{2.9}$$

where $u = [F_x^D, F_y^D]^T$ and boundary conditions are:

$$J_0 z(0) = z_0\,, \quad J_T z(T) = z_T \tag{2.10}$$

together with constraints on states:

$$a_1 \le z(t) \le a_2 \tag{2.11}$$

and quadratic constraints on controls

$$a_3 \le R_1 u + u^T R_2 u + \le a_4 \tag{2.12}$$

where the matrices J_0 and J_T are determined by Equations 2.5 and 2.6, and the matrices R_1 and R_2 are determined by the friction ellipse and the limitations on lateral acceleration from Equation 2.4. The optimal control problem is also regularized and augmented by adding a small energy term to the objective function.

$$\tilde{J}(z,u) = J(z,u) + w \int_0^T u^T u dt \tag{2.13}$$

w is a small number.

2.2 RECA by braking and steering

To investigate the potential of using the actuator configurations braking, steering and integrated braking and steering for RECA the optimal control problem defined in previous section is applied to variants of the RECA manoeuvre with varying initial vehicle speed.

Two different road friction surfaces are considered for RECA by steering. For the high friction road surface the lateral acceleration constraint due to rollover is active $(\max(a_y) = a_{y,\max},\ \mu\, g > a_{y,\max})$ but for the low friction road surface the friction of the road surface is not enough to reach the rollover limit $(\max(a_y) < a_{y,\max},\ \mu\, g < a_{y,\max})$.

For all configurations the critical manoeuvre for RECA is determined by the minimum required longitudinal distance:

$$J = X(T). \tag{2.14}$$

Three actuator configurations are considered:

- *Braking (B)*: Braking only using the brake actuators ($F_y^D = 0$). No lateral displacement for the manoeuvre ($Y_T = 0$).
- *Steering (S)*: Steering only with no braking ($F_x^D = 0$).
- *Integrated braking and steering (IBS)*: Braking and steering.

Numerical results are provided for a heavy vehicle in Figure 2.2 for low-μ road surfaces ($a_{x,\max} = a_{y,\max} = 2\ \mathrm{m/s^2}$), for braking ($a_{x,\max} = 6\ \mathrm{m/s^2}$) and hard braking ($a_{x,\max} = 7\ \mathrm{m/s^2}$), and also steering on the rollover limit ($a_{y,\max} = 3.6\ \mathrm{m/s^2}$) on high-$\mu$ road surfaces. For all numerical results the following input data are used: $X_0 = 0$, $Y_0 = 0$, $V_{x0} = 80\ \mathrm{km/h}, V_{y0} = 0, V_{yT} = 0$. For the steering only and the integrated braking and steering configuration the lateral displacement of a full lane change is used: $Y_T = 3\ \mathrm{m}$. Note that the delays due to the tyre relaxation lengths are neglected here, *i.e.* it is assumed that the force generation is instantaneous on the wheels ($\sigma_{x,y} = 0$). The problem is solved using the software PROPT [18] with 50 collocation points and the energy weighting factor $w = 0.0005$.

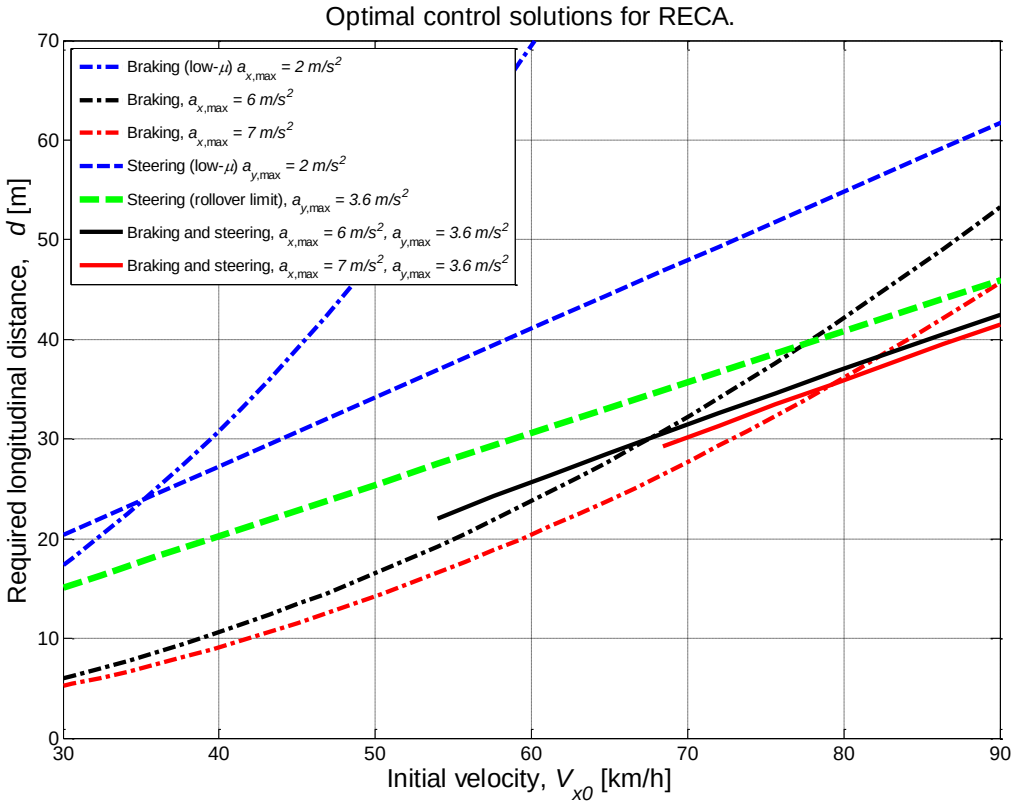

Figure 2.2 The required longitudinal distance versus initial longitudinal velocity for RECA by braking, steering and integrated braking and steering.

The optimal control results obtained for braking and steering actuator configurations in Figure 2.2 show that the required longitudinal distance for steering increases approximately linearly with velocity but proportional to the square of the velocity for the braking configuration. This gives a breakpoint velocity where steering becomes a better option for RECA. Considering the results for braking and steering on high-μ road the breakpoint velocity is $78\ \mathrm{km/h}$. It is also shown in Figure 2.2 that the integrated braking and steering actuator configuration moves the breakpoint down to $68\ \mathrm{km/h}$. This means that the integrated braking and steering actuator configuration has a wider velocity range where the required longitudinal distance with steering is less compared to braking only. Actually, due to the rollover risk, the breakpoint velocity occurs at a relatively high velocity for a truck, which

results in a quite narrow velocity window for RECA by steering. In return the relative sensitivity with respect to available road friction for given speed is less for steering compared to braking, see Figure 2.2. In summary, the conclusion can be made that the integrated braking and steering actuator configuration has the potential to improve the performance of RECA for a significant range of velocities.

In the coming subsections the sensitivity of the required longitudinal distance for variations of key characteristics of the RECA manoeuvre is investigated.

2.2.1 Lateral displacement

In previous section the required longitudinal distance for a critical manoeuvre is determined for various actuator configurations for a lateral displacement equivalent of a full lane change. In general the breakpoint velocity occurred for high velocities. The lateral displacement in the RECA manoeuvre is one of the key parameters. Large longitudinal distance provides a better opportunity to prevent the collision with mild manoeuvres while large lateral displacement causes a more aggressive manoeuvre. The driver comfort, and therefore the driver interaction, is also affected by harsh manoeuvres. This study shows the breakpoint velocity for manoeuvres with various lateral displacements in the manoeuvre for example if the lead vehicle in front is positioned with an offset with respect to the host vehicle or if the host vehicle is approaching a motorcycle. The result can also be used to determine the safety margin, used in Section 5.1.

Numerical results are provided for a heavy vehicle with steering on the rollover limit ($a_{y,\max} = 3.6\ \mathrm{m/s^2}$) a high-$\mu$ road surface with the same input data used in the previous section. The required longitudinal distance for various displacements is shown in Figure 2.3.

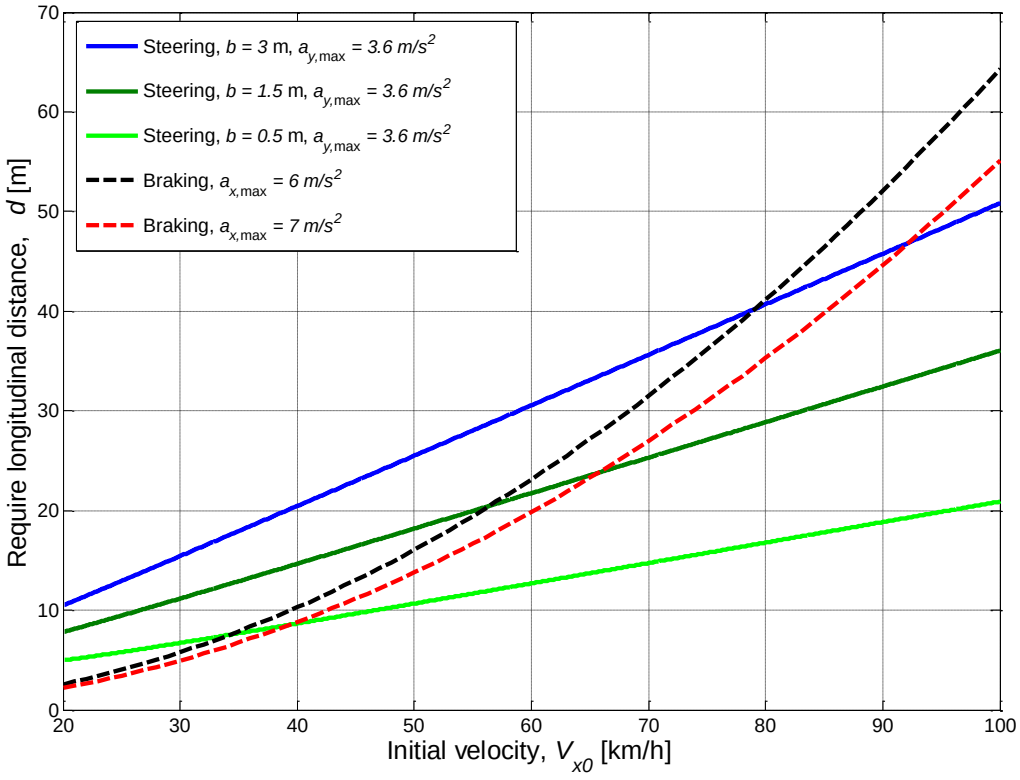

Figure 2.3 Required longitudinal distance versus initial velocity for given lateral displacements.

As illustrated in Figure 2.3, the breakpoint velocity is decreasing significantly with the lateral displacement.

2.2.2 Final course angle

The final lateral velocity of the vehicle in the RECA manoeuvre is another key parameter, which plays an important role in stabilizing and controlling the vehicle after the avoidance manoeuvre is completed. The final course angle is defined as:

$$\beta_T = \arctan\left(\frac{V_{yT}}{V_{xT}}\right). \qquad 2.15$$

This study investigates the effect on the required longitudinal distance by varying the final course angle. In the previous two sections it is assumed that there are no lateral velocity at the end of the manoeuvre (zero course angle). Here this constraint is released and the course angle is allowed to increase at the end of the manoeuvre to reduce the required longitudinal distance.

Numerical results are obtained for a heavy vehicle with steering on the rollover limit ($a_{y,\max} = 3.6\ \mathrm{m/s^2}$) on a high-$\mu$ road surface. The input data in the previous sections are used. The final lateral velocity V_{yT} is varied between 0 and $2\ \mathrm{m/s}$, which corresponds to a variation of the course angle between 0 and 5 degrees (Equation 2.15). The required longitudinal distance for various final course angles is shown in Figure 2.4.

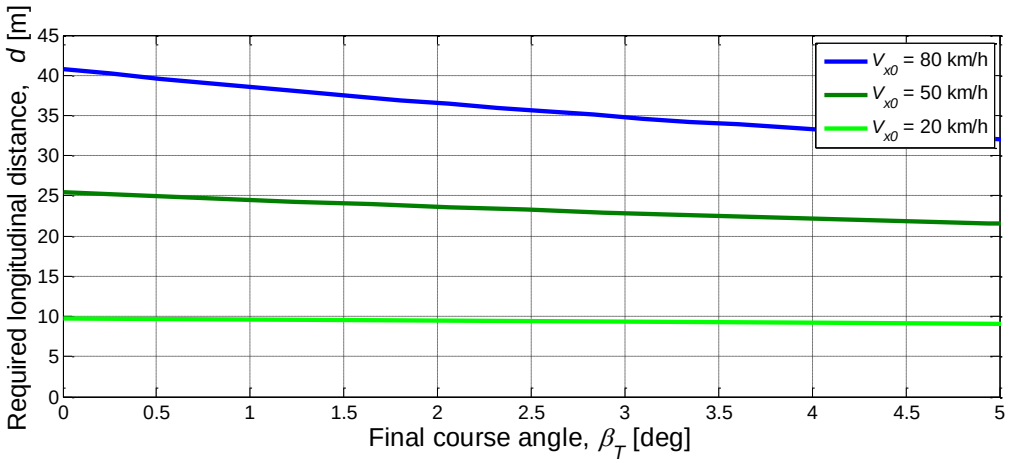

Figure 2.4 Required longitudinal distance versus final course angle for given initial velocity.

The required longitudinal distance is, as expected, decreasing with the final course angle for all given initial velocities. In particular for higher velocities the gain by allowing a nonzero final course angle is significant.

2.2.3 Variable braking versus constant braking

This subsection investigates the benefit of using variable braking compared to constant braking for the integrated braking and steering configuration. For constant braking the amount of braking does not change during the manoeuvre while implementing the variable braking, the braking force can be changed to obtain the optimal results. The problem formulation used in the previous subsections is also used here. Figure 2.5 bellow shows the numerical results.

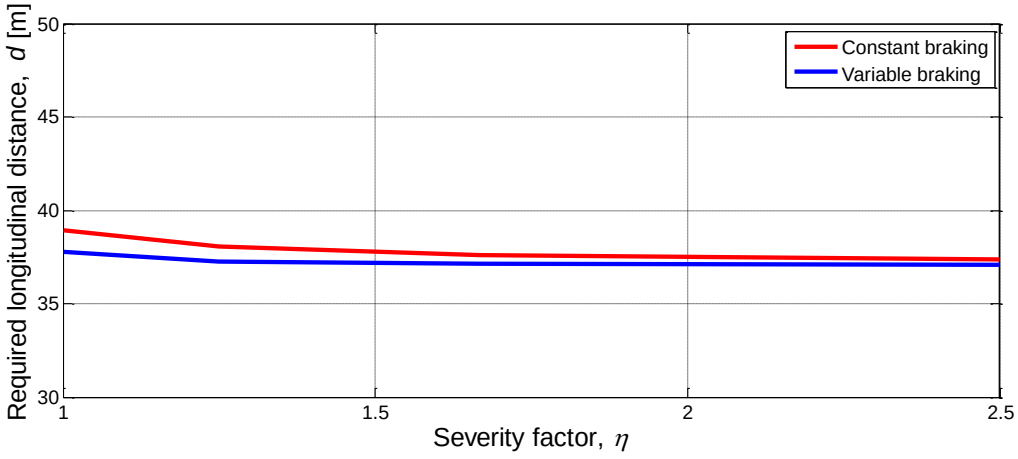

Figure 2.5 Required longitudinal distance for variable and constant braking.

In general, by using variable braking, the amount of required longitudinal distance is decreased, which means that the variable braking is more efficient. It can also be observed that for more severe manoeuvres with higher initial speeds (higher severity factor), there is small difference between constant and variable braking. However, the variable braking becomes more efficient compared to constant braking in less severe manoeuvres.

2.3 Manoeuvre severity

The objective of this section is to show the optimal integration of braking and steering in RECA considering the severity of the manoeuvre. The required longitudinal distance to stop the vehicle with the initial velocity of V_{x0} and road friction coefficient μ can be calculated as

$$c = \frac{V_{x0}^2}{\mu g}. \tag{2.16}$$

The maximum feasible lateral displacement with the initial speed of V_{x0} and road friction μ is denoted $b_{\max}$. The severity factor is defined as

$$\eta = \frac{c}{a}, \tag{2.17}$$

which is the ratio of the longitudinal distance required to stop the vehicle to the available longitudinal distance. To mitigate the consequences of a crash the objective here is to minimize the final longitudinal velocity

$$J = V_x(T). \tag{2.18}$$

Numerical results are obtained for a heavy vehicle with integrated braking and steering on the rollover limit ($a_{y,\max} = 3.6\ \mathrm{m/s^2}$) on a high-$\mu$ road surface. Here, it is assumed that the lateral displacement is 75% of the maximum feasible lateral displacement, which gives a challenging manoeuvre in terms of lateral displacement but still leaves room to optimize the integration of braking and steering to slow the vehicle down. The initial and final condition are defined as follows: $X_0 = 0,\ Y_0 = 0,\ V_{x0} = \sqrt{\eta\mu g a},\ V_{y0} = 0,\ Y_T = 0.75 b_{max},\ V_{yT} = 0.$

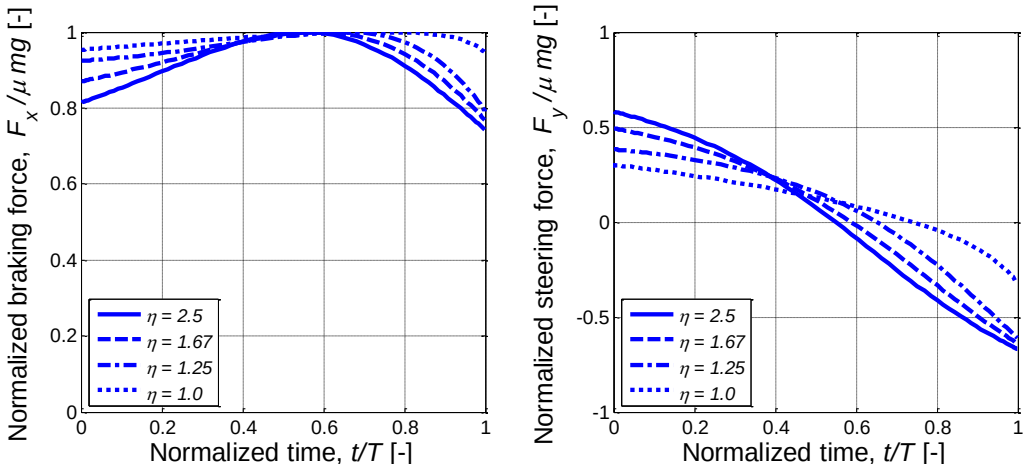

Figure 2.6 Integrated braking and steering for given maneuver severity.

It is observed from the results that for more severe manoeuvres, the optimal way of integrating braking and steering is to steer more in the beginning. This is because for a certain manoeuvre severity the last point of steer is defined by the most severe manoeuvre, where collision avoidance by steering can be applied.

It can also be concluded from these results that if the decision making part of the collision avoidance system is hesitating about how to combine the path and speed control due to inaccuracies, sensor problems, lack of data *etc.* it is probably beneficial to brake at the beginning until more information is available and the severity of the manoeuvre is known. Consequently, if the manoeuvre is not severe the vehicle has not lost any opportunity by reducing the speed and going into a less severe manoeuvre. On the other hand, if the manoeuvre is severe there will be two possible scenarios. Firstly, assuming that the vehicle has not passed the last point of steer, braking can be helpful since last point of steer is postponed by reducing the speed. Secondly, if the vehicle has passed the last point of steer,

pure steering configuration will not be helpful to avoid the accident and braking or integrated braking and steering are the only available options. Consequently, it may be possible either to stop the vehicle before the obstacle depending on velocity of the vehicle or to avoid the vehicle with integrated braking and steering intervention. Figure 2.2 shows when braking is better than steering in terms of required longitudinal distance. For the velocities where braking is worse than steering, there is no chance to stop the vehicle before the obstacle since the steering cannot perform the manoeuvre either. Nevertheless the accident is mitigated by braking and reducing the speed. It can be concluded that braking is very often a good initial action if the required information to take the optimal action is not available.

3 Heavy vehicle system dynamics

Simulation of the path stability control function for the prioritized use cases requires a heavy vehicle system dynamics model. In order to investigate the integration of steering and braking for collision avoidance manoeuvre, it is necessary to include both steering and braking in the model to well provide the possibility of a handling study with path stability control. The model here is partially borrowed and modified from [19]. It is verified through a comparison with logged data from an experiment, which is presented in Chapter 6.

3.1 Relevant assumptions

For the handling studies of a heavy vehicle in planar motion, longitudinal and lateral displacements in addition to yaw angle are necessary to study the path during a manoeuvre. Moreover, relatively high centre of gravity (CG) for a truck results in a considerable amount of load transfer during different manoeuvres, and explains the importance of including the role angle in the model. Therefore a two track four degrees of freedom (4DOF) model is required. Moreover, there are also simplifications made as below:

- Pitch dynamics is not modelled. In fact, yaw and roll motion together influence the pitch dynamics due to the gyroscopic effect. Longitudinal load transfer is calculated by assuming a rigid vehicle, *i.e.* suspension locked for pitch motion, and cross terms consisting of roll, yaw, and their rates are not considered.
- Neither the aerodynamic drag nor the effect of possible side winds are modelled.
- Suspension springs and dampers are assumed to behave linearly for the whole range of roll angles and roll rates.
- In a tandem axle group, longitudinal force and torque on one axle influences the vertical load on the other axle. This is due to the measures taken to distribute the load on each axle of the tandem group in a predefined ratio on uneven surfaces. In this study, it is assumed that the torque reaction rods are designed properly so they counteract such an additional vertical load transfer and cancel that effect.
- The steering angles of the left and right wheels on the first axle are assumed to be the same. The steering ratio is assumed to be constant. The lumped elasticity in the steering system is assumed to be linear.
- Ladder chassis is assumed to be rigid. In reality, truck chassis is made of so-called profiles with *open* cross-sections. Since this profiles are torsionally flexible and relatively rigid against bending, the overall chassis structure can easily be twisted. This is sometimes desired for trucks to better suit the road profile. As expected It also affects the lateral load transfer, but it is not considered.
- Rotating wheels are not simulated, and tyre rolling resistance is neglected.
- A linear reduction is assumed for the adhesion coefficient between the tyre and the ground with respect to the increasing normal load.

3.2 Planar motion of the heavy vehicle

A schematic planar sketch of the heavy vehicle together with the most important tyre forces, and steering angles, are shown in Figure 3.1 using ISO coordinate system.

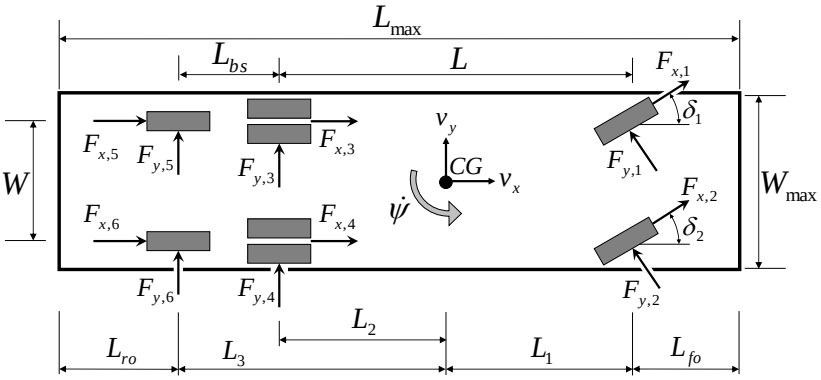

Figure 3.1 Schematic planar sketch of the 6×2 truck.

The gross dimensions L_{max} and W_{max} are particularly important for collision avoidance manoeuvres. $F_{x,n}$ and $F_{y,n}$ represent longitudinal and lateral tyre forces respectively, measured in the coordinate system fixed on the n^{th} wheel. v_x and v_y are longitudinal and lateral speed of the vehicle and $\dot{\psi}$ represents yaw rate. Finally, δ_n is steering angle of n^{th} wheel. Note that only the front axle is steered. However, wheels on the other axles will also have small steer angles, which are not shown but will be discussed later.

Since pitch dynamics and cross terms due to yaw, roll, and their time derivatives are neglected, equations of motion will be simplified as follows. In longitudinal direction (x) one can write:

$$\Sigma F_x = ma_x\,, \qquad a_x = \dot{v}_x - v_y\dot{\psi} \tag{3.1}$$

$$\Rightarrow \sum_{n=1}^{6}\left(F_{x,n}\cos\delta_n - F_{y,n}\sin\delta_n\right) = m\left(\dot{v}_x - v_y\dot{\psi}\right) \tag{3.2}$$

where m represents the mass of the heavy vehicle.

In lateral direction (y) the equation will have the form below

$$\Sigma F_y = ma_y, \qquad a_y = \dot{v}_y + v_x\dot{\psi} \tag{3.3}$$

$$\Rightarrow \sum_{n=1}^{6}\left(F_{y,n}\cos\delta_n + F_{x,n}\sin\delta_n\right) = m\left(\dot{v}_y + v_x\dot{\psi}\right). \tag{3.4}$$

Finally, for the moments in the third direction (z) equations can be written as

$$\Sigma M_z = I_{zz}\ddot{\psi} \tag{3.5}$$

$$\Rightarrow \sum_{n=1}^{6}\left(\left(F_{x,n}\sin\delta_n + F_{y,n}\cos\delta_n\right)l_n - \left(F_{x,n}\cos\delta_n - F_{y,n}\sin\delta_n\right)w_n\right) = I_{zz}\ddot{\psi}, \tag{3.6}$$

where I_{zz} is the mass moment of inertia, and l_n and w_n are longitudinal and lateral positions of n^{th} wheel in the coordinate system fixed to the body, respectively.

3.3 Roll of the sprung mass

It is necessary to consider the roll of the sprung mass since it induces a significant amount of lateral load transfer in a heavy vehicle. Figure 3.2 shows the free body diagram of the sprung mass in dynamic equilibrium where inertial force and moment are shown in gray block arrows.

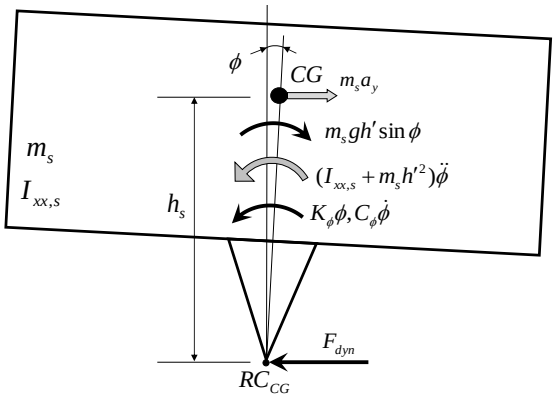

Figure 3.2 Free body diagram of the sprung mass.

Note that the static equilibrium condition is taken as the reference; hence the vertical forces that cancel each other are not shown. The location of the centre of gravity for the sprung mass (m_s) is assumed to be the same as the location of the centre of gravity for the whole vehicle since $m_s/m = 0.9 \approx 1$. Roll acceleration ($\ddot{\phi}$) can be calculated using differential equation expressing the roll dynamics of the sprung mass. Considering Figure 3.2, summing the moments about the RC_{CG}, using the parallel axis theorem (Steiner theorem), and assuming small angles (roll angles do not exceed 10°), one can write

$$\Sigma M_{RC_{CG}} = 0, \tag{3.7}$$

$$\Longrightarrow \left(I_{xx,s} + m_s {h_s}^2\right)\ddot{\phi} - m_s g h_s \phi + K_\phi \phi + C_\phi \dot{\phi} - m_s h_s \left(\dot{v}_y + v_x \dot{\psi}\right) = 0, \tag{3.8}$$

where $I_{xx,s}$ is the mass moment of inertia around x axis for the sprung mass, and K_ϕ and C_ϕ are roll stiffness and roll damping, respectively.

3.4 Lateral and longitudinal load transfer

Roll of the sprung mass induces load transfer on all axes as shown for i^{th} axle as in Figure 3.3. Note that the static equilibrium condition is taken as the reference; hence the vertical forces that balance each other are not shown.

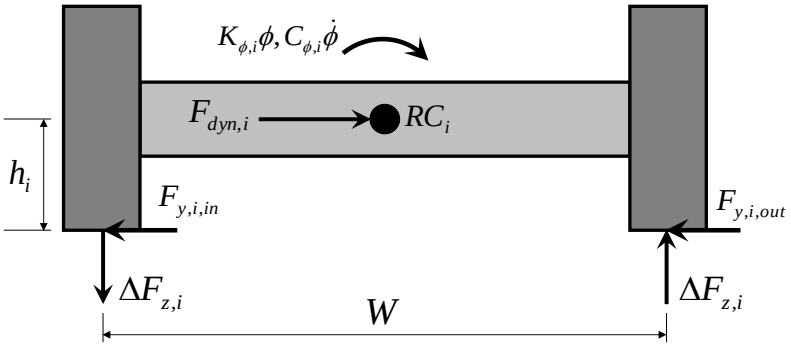

Figure 3.3 Free body diagram of the i^{th} axle.

$F_{dyn,i}$ represents sum of the forces on the axle due to dynamical state of the axle, and can be determined using Equation 3.8. According to Figure 3.3 and ignoring the mass of the axle, it can be calculated as

$$F_{dyn,i} = F_{y,i,in} + F_{y,i,out}. \tag{3.9}$$

If n denotes the tyre corresponding to $F_{y,i,in}$ (or $F_{y,i,out}$), they can be calculated as

$$F_{y,i,in} = F_{x,n} \sin\delta_n + F_{y,n} \cos\delta_n. \tag{3.10}$$

Assuming that none of the wheels is lifted, the lateral load transfer on i^{th} axle ($\Delta F_{z,lat,i}$) could be determined by summing moments around RC_i that results in

$$\Delta F_{z,lat,i} = \frac{K_{\phi,i}\phi + C_{\phi,i}\dot{\phi} + h_i F_{dyn,i}}{W}. \quad 3.11$$

Note that additional effect of the acceleration term $\dot{\phi}h'$ on the vertical forces is neglected. In order to calculate the load transfer on tandem axles, some assumptions and definitions are required. Tandem axles are designed in a way that they prevent one axle from being overloaded and especially causing damage to the road when negotiating uneven surfaces [20]. A simple way to achieve this is to use scale-beam principle [21] where the two axles are connected to a big leaf spring and the leaf spring is mounted on the chassis in a way that it can pivot and prevent any axle in this group from losing contact with the road. This design matches with the truck of interest in this study. By using theoretical wheelbase (L_t) as in [22], the three-axle vehicle can be reduced to a equivalent two-axle vehicle in the same static equilibrium. The theoretical wheelbase can be calculated as

$$L_t = L + \frac{F_{z0,3}}{F_{z0,2} + F_{z0,3}}(L_3 - L_2), \quad 3.12$$

where $F_{z0,i}$ is the static load on the i^{th} axle. Correspondingly, the centre of gravity from front axle can be determined as

$$L_1 = \frac{F_{z0,2} + F_{z0,3}}{\sum_i F_{z0,i}} L_t. \quad 3.13$$

The longitudinal load transfer can now be calculated for the equivalent 2-axle vehicle and once the total longitudinal load transfer on the tandem axle is calculated, the longitudinal load transfer on the both second and third axle could be determined by using the moment equilibrium, *i.e.* they are proportional to the static loads on the axles mentioned. The mathematical expressions are as

$$\Delta F_{z,lon,1} = -ma_x \frac{h}{L_t}, \quad 3.14$$

$$\Delta F_{z,lon,2} + \Delta F_{z,lon,3} = ma_x \frac{h}{L_t}. \quad 3.15$$

Using Equation 3.15 and writing static equilibrium about pivot point, load transfer on tandem axles can be derived as

$$\Delta F_{z,lon,2} = ma_x \frac{h}{L_t}\left(\frac{F_{z0,2}}{F_{z0,2} + F_{z0,3}}\right), \quad 3.16$$

$$\Delta F_{z,lon,3} = ma_x \frac{h}{L_t}\left(\frac{F_{z0,3}}{F_{z0,2} + F_{z0,3}}\right). \quad 3.17$$

Distributing the longitudinal load transfer of one axle equally among the wheels on that axle results in the load transfer for each individual wheel on the axle.

In the vehicle data, the centre of gravity position is not directly given. Instead, roll centre height at each axle and the height of CG above the roll axis are provided. Here, it is assumed that the aforesaid pivot point absorbs all the lateral forces from the wheels on the second and the third axles, thus the roll centre height for the tandem axle group becomes the same as the height of the pivot point. In a typical 3-axle Volvo truck, roll centre heights at the 2nd and the 3rd axles are usually equal ($h_2 = h_3$) and therefore RC height for the tandem group is equal to one of them or the average of them. Consequently, the CG height could be calculated as

$$h = h_1 + \left(\frac{h_2 + h_3}{2} - h_1\right)\frac{L_1}{L_t} + h_s. \quad 3.18$$

3.5 Slip angle and net steering angle

The calculation of tyre forces requires determination of slip angle of the individual wheels. The slip angle of each wheel (α_n) can be calculated as

$$\alpha_n = \delta_n - \arctan\left(\frac{v_{y,n}}{|v_{x,n}|}\right), \quad n = 1,2,\dots 6, \tag{3.19}$$

where δ_n is the steering angle of n^{th} wheel, and $v_{x,n}$ and $v_{y,n}$ are longitudinal and lateral speed at contact patch. The absolute value of the longitudinal speed of each wheel has to be taken into account since the direction of the tyre force is only determined by the direction of the lateral speed (regardless of the direction of the longitudinal speed) at contact patch. In comparison with the vehicle speed, track width and yaw rate induce an additional effect on the speed of the tyre contact patch. Taking this effect into account, Equation 3.19 can be written as

$$\alpha_n = \delta_n - \arctan\left(\frac{v_y + l_n\dot{\psi}}{|v_x - w_n\dot{\psi}|}\right), \quad n = 1,2,\dots 6. \tag{3.20}$$

Note that the same slip angles are assumed for the tyres on the dual wheel combination on second axle. In this study, only the front axle is assumed to be steerable. However, this does not mean that the steering angle for the wheels on the either second or third axle are zero. Due to the kinematics and elasticity of the axle/suspension system, wheel/axles deflect in the presence of the lateral forces, longitudinal forces, realigning moments, and sprung mass roll. The steering angle on all axles are determined after taking the kinematic/elastokinematic effects into consideration. Three main effects can be listed as roll steer, lateral force steer, and aligning moment steer. Roll steer is usually the dominant effect for a heavy vehicle. It is caused by one side of the axle moving forward and the other side of the axle moving backward due to the asymmetric deflection of the leaf springs and/or the geometric location and also the kinematics of the suspension links (including the steering links). In this study, only the roll steer is considered because of its dominance. Roll steer is normally a nonlinear function of the roll angle, but due to small roll angles, it is assumed to be linear. A roughly estimated roll steer coefficients (ε_n) have been acquired from [23] for the first axle towards understeer, and for the second and the third axles towards oversteer. In general, when the suspension is concerned, the wheel deflections towards toe-in are assigned to be positive, hence the roll steer coefficient is positive if the wheel deflection is towards toe-in for a positive roll angle. Note that this sign convention is used while expressing the wheel angles in the report. The wheel angles of the first axle can be determined as

$$\delta_n = \delta_{r,n} + (-1)^n \varepsilon_n \phi\,; \quad n = 1,2 \tag{3.21}$$

where $\delta_{r,n}$ is called *reduced* road wheel angle of n^{th} wheel and is the steering angle that is transmitted to the wheel. The commanded steering wheel angle input is transmitted to the wheels via a recirculation ball steering gearbox and corresponding steering links. In general, the ratio between the steering wheel angle and the road wheel angle is not constant. However, here the steering ratio (i_s) is assumed to be constant. There are also some losses while transmitting the steering wheel motion into the road wheel motion due to the elasticity of the whole steering system. When the tyres generate side forces, these forces compress the whole system, and lead to a reduction in the wheel angle. This effect is nonlinear in reality, but a linear relation is assumed in this study. The lumped compliance for the system (c_δ) is taken from [23]. The reduced road wheel angles can be determined as

$$\delta_{r,1} = \delta_{r,2} = \frac{\delta_{SWA}}{i_s} - c_\delta\left(F_{y,1} + F_{y,2}\right), \tag{3.22}$$

where δ_{SWA} is steering wheel angle. Since wheels on the tandem axles are not steered, the corresponding reduced road wheel angles are equal to zero, and the wheel angle for them can be calculated as

$$\delta_n = (-1)^n \varepsilon_n \phi\,; \quad n = 3,4,5,6. \tag{3.23}$$

In this study, the steering command is provided by the steering actuator. In order to include a simple model of the steering system, a first order system is used that can be expressed as

$$\dot{\delta} + \frac{1}{\tau}\delta = \delta^{\mathrm{act}} \tag{3.24}$$

where δ^{act} is the steering angle provided by the steering actuator, and τ is the time constant.

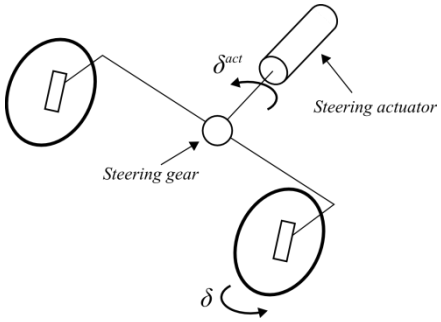

Figure 3.4 Schematic view of the steering system.

3.6 Tyre force generation

Tyre behaviour is modelled using the Magic Tyre Formula [24] as can be written as

$$F_y^{\mathrm{MF}} = D\sin\big(C\arctan\big(B\alpha - E(B\alpha - \arctan(B\alpha))\big)\big) \tag{3.25}$$

More explanation and details, in addition to the other relevant approximations and assumption about friction coefficient and tyre stiffness can be found in Appendix A.

The Magic Tyre Formula provides the steady state tyre lateral force. However, it is known that in practice, a tyre must translate in order to generate slip angle thus build up side force. This means that the side force build-up is not instantaneous since some time and translation distance are needed to stretch the tyre components. In order to model the transient tyre force generation, the concept of *relaxation length* is used in a first order approximation for the tyre lateral force build-up, as

$$\frac{\sigma_y}{v_x}\dot{F}_y + F_y = F_y^{\mathrm{MF}}, \tag{3.26}$$

where σ_y is the lateral relaxation length, and v_x is the longitudinal speed at the contact patch of the tyre. Note that the differential equation above is not linear because v_x is not constant. In addition, the relaxation length is shown to be changing with slip angle [25]. However, σ_y is assumed to be constant here and its value can be found among vehicle data in Table of notations. The same concept also applies to the longitudinal force build-up. The gradual first order change of the longitudinal tyre forces can be expressed as

$$\frac{\sigma_x}{v_x}\dot{F}_x + F_x = F_x^{\mathrm{rim}}, \tag{3.27}$$

where σ_x is the longitudinal relaxation length that is treated same as the lateral relaxation length here, and may be found among vehicle data in Table of notations. The input to the differential equation above would be the brake force that may be demanded by a controller. Note that the rim force, F_x^{rim}, is a fictitious internal force acting on the rim that results in the same tyre force in the steady state.

4 Path and speed control

A collision avoidance manoeuvre requires a generic path and speed control system that can plan a reference path for any given use case, and control the vehicle to follow the reference path until the manoeuvre is completed. A schematic overview of such a path and speed control system is shown in Figure 4.1. Based on a given use case, a reference path is generated during path planning for the heavy vehicle to follow. Employing the reference path, reference inputs required for the interaction with the heavy vehicle model can be calculated for both feedforward and feedback controllers. Therefore at the intervention start point, the heavy vehicle is expected to start the collision avoidance manoeuvre suitable for the existing use case. Building blocks of the entire path and speed control system are explained in this chapter.

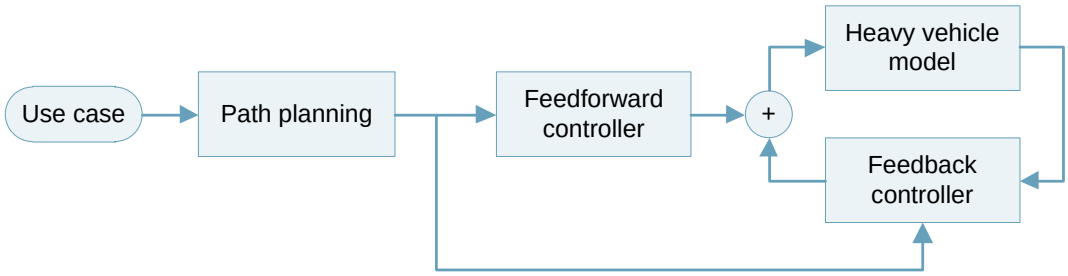

Figure 4.1 Schematic overview of a generic path and speed control system.

4.1 Roll stability

Due to relatively high centre of gravity in a truck, it is very prone to rollover in severe manoeuvres. Therefore rollover is one of the most important issues to consider in handling studies of a heavy vehicle, and is the first constraint to consider in path planning. To obtain a criterion for rollover, it is sufficient to keep the vehicle in steady state during the manoeuvre. This can be interpreted as limiting the maximum lateral acceleration of the heavy vehicle. The maximum allowed lateral acceleration of a heavy vehicle can be calculated using the equations of motion. Using Equation 3.8 one can rewrite Equation 3.11 for steady state and considering that rollover first occurs when the load transfer is equal to the static load on the front outer wheel, the maximum lateral acceleration can be determined as

$$a_{y,\max} = \frac{WF_{z0,1}}{\frac{K_{\phi,1} m h_s}{\left(K_{\phi,1}+K_{\phi,2+3}\right)-mgh_s}+m_1 h_1}, \tag{4.1}$$

where, $K_{\phi,2+3}$ is the roll stiffness of a single axle equivalent to the tandem axle, and m_1 is the mass distributed on the front axle.

4.2 Steady state cornering

In order to calculate the steering angle on the wheel for steady state cornering, equations of motion (3.1-3.6) can be used to reduce the two-track 3-axle heavy vehicle model to an equivalent one-track bicycle model [26]. Then the steady state steering angle for equivalent bicycle model can be determined as

$$\bar{\delta} = \frac{L_e}{R} + K_e \frac{a_y}{g}, \tag{4.2}$$

where, $\bar{\delta}$ is the steady state steering angle, R is the radius of the path curvature, L_e and K_e are equivalent wheelbase and equivalent understeer coefficient, respectively. The equivalent wheel base can be calculated as

$$L_e = L + L_{bs}\frac{C_1C_3(L+L_{bs})+C_2C_3L_{bs}}{C_1C_2L+C_1C_3(L+L_{bs})}, \quad 4.3$$

where L is the distance between the first and the second axle, and L_{bs} is the bogie spread as both can be found in Figure 3.1. Cornering stiffness of the first, second, and the third axle are represented by C_1, C_2, and C_3 respectively. The equivalent understeer coefficient can be determined as

$$K_e = -m\frac{C_1L_1-C_2L_2-C_3L_3}{C_1C_2L+C_1C_3(L+L_{bs})}, \quad 4.4$$

where m is the vehicle mass and L_1, L_2, and L_3 are distance between centre of gravity, CG, and the first, second, and the third axle, respectively, as shown in Figure 3.1.

4.3 Path planning

Path planning is performed in advance of an intervention. During path planning, a reference path should be generated that can provide continuous and smooth profiles for the vehicle position, velocity, and acceleration. Simplicity and flexibility are also necessary in path planning to easily generate the reference path for different use cases. In this study, a fifth order polynomial is considered and examined to generate the reference path. The fifth order polynomial may be defined as

$$Y_{\text{ref}}(X) = \sum_{j=0}^{5} c_i X^i \quad 4.5$$

where X is the longitudinal position of the vehicle, Y_{ref} is the lateral position on the reference path, and c_i represents coefficients of the fifth order polynomial. In order to calculate coefficients, initial and final boundary conditions are required. The vehicle motion at the beginning and end of a desired manoeuvre, can be interpreted as initial and final boundary conditions of the required reference path. Knowing the boundary conditions, coefficients can be calculated analytically as described in Appendix B. An example set of coefficients that are calculated for a path corresponding to a single lane change with longitudinal distance of d and lateral displacements of b, are given in Table 4.1.

Coefficients		c_0	c_1	c_2	c_3	c_4	c_5
Values	Parametric	0	0	0	$10\frac{b}{d^3}$	$15\frac{b}{d^4}$	$6\frac{b}{d^5}$
	$d = 50$ m, $b = 3$ m	0	0	0	$2.4e-4$	$-7.2e-6$	$5.76e-8$

Table 4.1 Coefficients of an example fifth order polynomial corresponding to a single lane change.

However, not all fifth order polynomials are feasible paths for the heavy vehicle. On the one hand, the controller should operate within the bandwidth of the steering actuator. Otherwise, the actuator cannot provide what the controller demands that are based on the reference path for performing the manoeuvre. For example, the performance of the steering actuator in generating the steering wheel angle and its rate, is bounded due to both mechanical limitations and safety requirements for the interaction with the driver. On the other hand, it should be possible for the heavy vehicle to follow the reference path safely without skidding or rolling over, *i.e.* the vehicle should stay within its manoeuvrability limits. Therefore, the feasibility of the manoeuvre needs to be ensured by comparing all involving parameters with the corresponding limits for all points along the reference path. For this purpose, the equivalent steady state bicycle model described in Section 4.2 is used to determine all necessary parameters as functions of X. To satisfy the constraints, it is enough to keep all

involving parameters below their limits. The steering actuator constraints that are taken into account in this study, can be checked as

$$\left|\bar{\delta}(X)\right| \le \delta_{\max}, \qquad \left|\dot{\bar{\delta}}(X)\right| \le \dot{\delta}_{\max}, \qquad |\bar{T}(X)| \le T_{\max}, \tag{4.6}$$

where $\bar{\delta}$ is the steering angle, $\dot{\bar{\delta}}$ is the steering angle rate, and $\bar{T}$ is the steering actuator torque, all in the steady state condition.

The manoeuvrability of a heavy vehicle on a high friction surface is, in general, limited by the rollover threshold rather than the tyre's capacity to generate side force. Thus lateral acceleration shall be kept bellow rollover threshold, estimated from Equation 4.1, to eliminate any risk of rollover;

$$\left|a_y(X)\right| \le a_{y,\max}. \tag{4.7}$$

In order to calculate a_y as a function of X along the reference path, in the steady state condition one can write

$$a_y(X) = \kappa_{\mathrm{ref}}(X)V^2, \tag{4.8}$$

where V is the vehicle speed that is constant in the steady state. It is worth to notice that Equation 4.8 indicates strong speed dependence for lateral acceleration constraint, and consequently for the whole manoeuvre. κ_{ref} is the curvature of the reference path that can be calculated as a function of X as

$$\kappa_{\mathrm{ref}}(X) = \frac{{Y_{\mathrm{ref}}}''}{\sqrt{\left(1+{Y_{\mathrm{ref}}}'^2\right)^3}}, \quad R_{\mathrm{ref}} = \frac{1}{\kappa_{\mathrm{ref}}} \tag{4.9}$$

where ${Y_{\mathrm{ref}}}'$ and ${Y_{\mathrm{ref}}}''$ are the first and second derivatives of Y_{ref} with respect to X, and can be calculated using Equation 4.5.

The critical path is the shortest feasible reference path that satisfied all conditions stated in Equations 4.6 and 4.7. In order to determine the critical path, all constraints shall be examined for If any of the constraints was violated, then boundary conditions need to be changed to calculate a new path. Among all boundary conditions, it is only possible to change final longitudinal position, since the other are requirements that are either determined by the dynamical state of the vehicle or defined by the use case. Increasing the longitudinal distance consequently allows for a less severe manoeuvre. Then constraints will be checked again and the iteration will be repeated until all constraints are satisfied and the critical path is found with the required longitudinal distance, d_c. A schematic overview of the general procedure is shown in Figure 4.2 and Figure 4.3, and values used for the constraints can be found in Table 5.1.

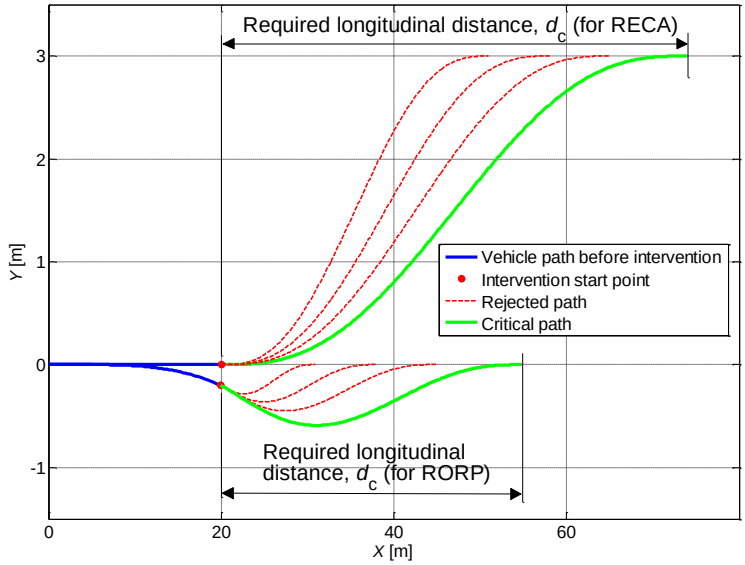

Figure 4.2 Schematic overview of the fifth order polynomial path planning for RECA and RORP on a straight road.

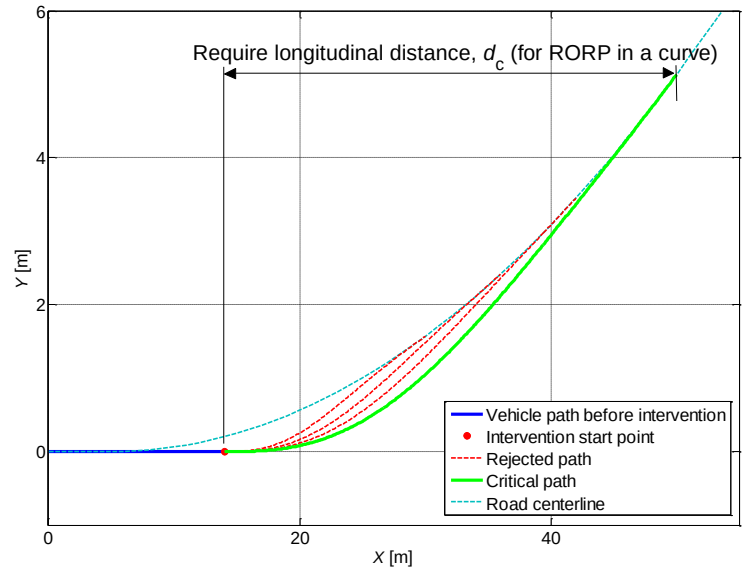

Figure 4.3 Schematic overview of the fifth order polynomial path planning for RORP in a curve.

In real truck experiment or in collision avoidance applications, it is desirable to consider a safety margin. The safety margin can be achieved by increasing the required longitudinal distance. In other words, increasing the required longitudinal distance for a manoeuvre is equivalent to adding safety margin, ζ, to the critical manoeuvre, as

$$\zeta = \frac{d - d_c}{d_c} \times 100 \qquad 4.10$$

where d represents required longitudinal distance.

The main advantage of the fifth order polynomial is that it provides a smooth and continuous path profile. Therefore, this path can be used to calculate the feedforward steering input, and also other reference values for the feedback controllers. In this study, the fifth order polynomial is used for all simulations with the heavy vehicle model presented in Chapter 5. It is also used for the experiments that are presented in Chapter 6.

4.4 Controller objectives and performance measures

In order to evaluate the performance of the path stability controller, some parameters are defined as performance criteria. Lateral position error is defined as

$$e_Y = Y_{\text{ref}} - Y, \tag{4.11}$$

where Y_{ref} and Y are the reference and actual lateral position of the vehicle, respectively. The latter is the measured value that, if unavailable or unreliable, needs to be estimated. It is necessary to mention that, unless specified, the CG position of the heavy vehicle, including both lateral and longitudinal direction, is intended in this work whenever position is discussed. However, in order to make sure of collision avoidance in RECA, it is necessary to check the distance between the heavy vehicle (host vehicle) and the obstacle (lead vehicle), specifically when their longitudinal position are close to each other. Since this distance, in addition to constant vehicle dimensions, is dependent on both position and heading angle, it is enough to keep the lateral position error and heading angle error under certain limits to make sure of collision avoidance. The heading angle error is defined as

$$e_\psi = \psi_{\text{ref}} - \psi, \tag{4.12}$$

where ψ_{ref} and ψ are the reference and actual heading angle of the vehicle, respectively. ψ is also a measured value that, if unavailable or unreliable, needs to be estimated. The reference heading angle is directly calculated using the geometry of the reference path profile and zero side slip assumption, as

$$\psi_{\text{ref}} = \arctan(Y'_{\text{ref}}), \tag{4.13}$$

where Y'_{ref} is derivative of the Y_{ref} with respect to X, can be calculated using Equation 4.5. Taking derivatives of the equation above and using the chain rule, $\dot{\psi}_{\text{ref}}$ can also be calculated as

$$\dot{\psi}_{\text{ref}} = \frac{d\psi_{\text{ref}}}{dt} = \frac{d\psi_{\text{ref}}}{dX}\frac{dX}{dt} = \frac{Y''_{\text{ref}}}{1 + {Y'_{\text{ref}}}^2}\dot{X}, \quad \dot{X} = v_x \cos\psi - v_y \sin\psi \tag{4.14}$$

where $\dot{X}$ can be approximated as equal to the vehicle speed if the vehicle lateral speed could be neglected and ψ would be small enough.

The required amount of the steering actuator torque, T, and its rate, $\dot{T}$, in order to perform the manoeuvre are also taken into consideration as performance measures. These parameters basically determine the requirements for the steering actuator and therefore are limited by the actuator limitations in generating the torque and also the torque rate. Finally, the lateral jerk, i, is defined as time derivative of the lateral acceleration; $\dot{a}_y$. These values shall be compared to their maximum allowed values as stated in tables of simulation results in Chapters 5.

4.5 Steering control

The path controller objective is to minimize the both path and heading angle errors while maintaining the both manoeuvrability and roll stability during the collision avoidance manoeuvre by steering. The main reference for this controller is the reference path generated by path planning procedure. Based on the reference path and dynamical state of the vehicle at the intervention start point, a feedforward controller can calculate suitable feedforward steering input. A feedback controller also takes care of uncertainties, unmodeled dynamics, and neglected parameters to help the vehicle follow the reference path. Since the vehicle's response to the both steering and braking inputs is not instantaneous, controlling the vehicle based on the reference point, that it is just passed, cannot help the vehicle to follow the trajectory ahead, especially if the vehicle is moving at high speed. Therefore, a lookahead distance, which provides a reference point ahead of the vehicle is implemented. As described in the first chapter, it is also assumed that other necessary input information to

the controller, *e.g.* vehicle position, heading angle (yaw), and heading angle rate (yaw rate), will be measured by perception system and fused to collision avoidance functions, so becomes available for the controller. Otherwise, any missing or unreliable information should be estimated based on the available and reliable information.

4.5.1 Feedforward

When the reference path is generated during the path planning, the feedforward steering angle, δ_{FF}, can be calculated using the steady state steering wheel angle form Equation 4.2 and multiplying with steering gear ratio, i_{st}, as

$$\delta_{\mathrm{FF}} = i_{\mathrm{st}}\left(\frac{l_{\mathrm{e}}}{R_{\mathrm{ref}}} + K_{\mathrm{e}}\frac{a_{y,\mathrm{ref}}}{g}\right), \tag{4.15}$$

where $a_{y,\mathrm{ref}}$ and R_{ref} can be determined at the intervention start point, using Equation 4.8 and Equation 4.9, respectively.

4.5.2 Feedback

The feedback controller takes care of uncertainties, unmodeled dynamics, and neglected parameters that cannot be handled by feedforward controller. Since the main desire during the manoeuvre is to stay on the reference path, an ideal controller would need to directly control the vehicle position. Having the reference path as function of longitudinal position, it is enough to control the lateral position to control the vehicle position. Therefore, the vehicle can be expected to stay on the reference path if the lateral position is well controlled, and its error is eliminated. For this purpose, a PID control on the lateral position (Y) error is chosen that can be described as

$$\delta_{\mathrm{FB}}^{Y} = K_{PY}e_Y + K_{IY}\int e_Y d\tau + K_{DY}\dot{e}_Y, \tag{4.16}$$

where δ_{FB}^{Y} is the feedback steering angle, e_Y is the lateral position error, and $\dot{e}_Y$ is time derivative of the lateral position error. K_{PY}, K_{IY}, and K_{DY} are the PID controller gains that need to be determined through a specific procedure.

A PD controller on the yaw angle (ψ) error can also be described as below

$$\delta_{\mathrm{FB}}^{\psi} = K_{P\psi}e_\psi + K_{D\psi}\dot{e}_\psi, \tag{4.17}$$

where δ_{FB}^{ψ} is the feedback steering angle, e_ψ is the yaw angle error, and $\dot{e}_\psi$ is time derivative of the yaw angle error. $K_{P\psi}$ and $K_{D\psi}$ are controller gains that need to be determined through specific procedure. The total feedback steering angle is sum of feedforward and feedback steering angles as

$$\delta_{\mathrm{FB}} = \delta_{\mathrm{FB}}^{Y} + \delta_{\mathrm{FB}}^{\psi}. \tag{4.18}$$

The total steering input of the vehicle will then be:

$$\delta = \delta_{\mathrm{FF}} + \delta_{\mathrm{FB}}. \tag{4.19}$$

A schematic figure of the path controller is provided in Figure 4.4.

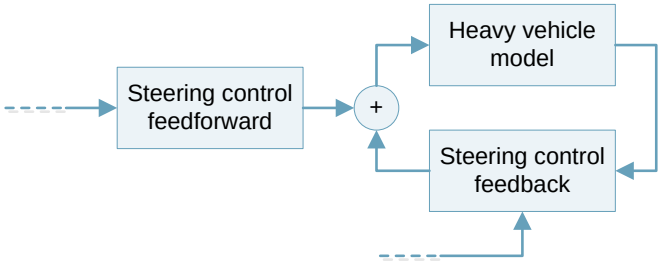

Figure 4.4 Schematic sketch of path stability controller.

4.5.3 Lookahead control

It is known that due to dynamics of the heavy vehicle, its response to both steering and braking demands are not instantaneous. This latency becomes critical in an emergency manoeuvre when milliseconds will count. In order to compensate for this latency, the controller is prepared to control the vehicle based on lookahead information.

Assuming the latency equal to lookahead time, t_{la}, the lookahead point is defined as an imaginary point fixed to the x-axis of the vehicle at a lookahead distance, d_{la}, from CG. Figure 4.5 shows a schematic representation of lookahead information.

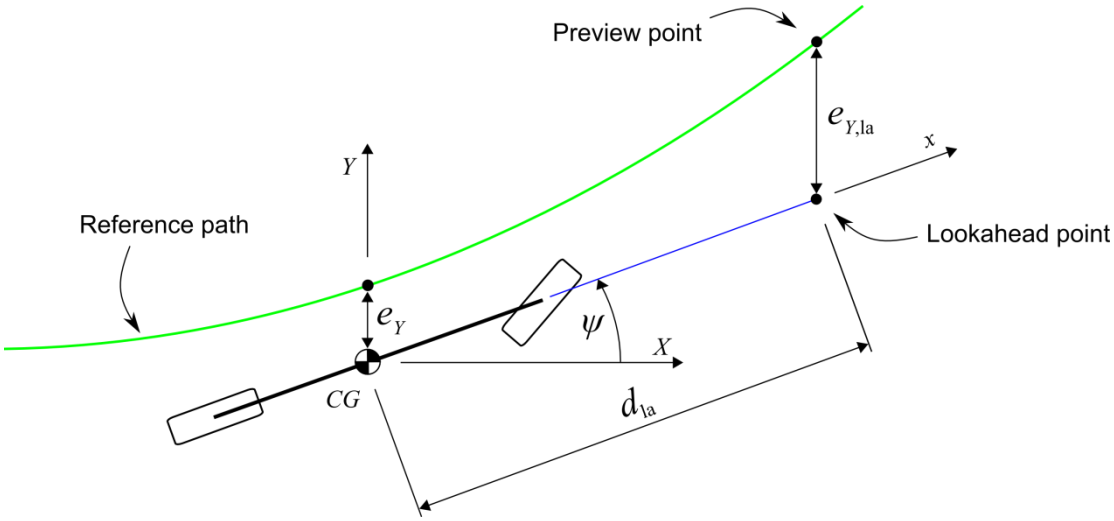

Figure 4.5 Lookahead information.

The lookahead distance is calculated using the vehicle speed, V, as

$$d_{\mathrm{la}} = V t_{\mathrm{la}}. \tag{4.20}$$

Then as input to the feedback controller, the lookahead error is defined as the error that is calculated at lookahead distance. The lateral position error at lookahead point, $e_{Y,\mathrm{la}}$, is calculated as

$$e_{Y,\mathrm{la}} = (Y_{\mathrm{ref}} - Y)_{X=X_{\mathrm{la}}} = Y_{\mathrm{p}} - (Y + d_{\mathrm{la}} \sin\psi), \tag{4.21}$$

where X_{la} is the longitudinal position of the lookahead point, and Y_{p} is the lateral position of the preview point that is a point on the reference path at longitudinal position of the lookahead distance, as shown in Figure 4.5. X_{la} can be calculated as

$$X_{\mathrm{la}} = X + d_{\mathrm{la}} \cos\psi. \tag{4.22}$$

Having the reference path function and X_{la}, Y_{p} can be calculated since it is also a function of X_{la}. Similarly, $\dot{Y}_{\mathrm{p}}$ can be calculated as a function of X_{la} using 4.14, and makes it possible to calculate the time derivative of the lateral position error as

$$\dot{e}_{Y,\mathrm{la}} = \left(\dot{Y}_{\mathrm{ref}} - \dot{Y}\right)_{X=X_{\mathrm{la}}} = \dot{Y}_{\mathrm{p}} - \left(\dot{Y} + d_{\mathrm{la}}\dot{\psi}\cos\psi\right). \quad 4.23$$

In order to include lookahead information in the feedback controller, e_Y and $\dot{e}_Y$ shall be replaced with $e_{Y,\mathrm{la}}$ and $\dot{e}_{Y,\mathrm{la}}$ in Equation 4.16 to calculate the feedback value. With a small angle assumption for yaw angle, Equations 4.21 and 4.23 can be written as4.23

$$e_{Y,\mathrm{la}} \approx Y_{\mathrm{p}} - (Y + d_{\mathrm{la}}\psi), \quad 4.24$$

$$\dot{e}_{Y,\mathrm{la}} \approx \dot{Y}_{\mathrm{p}} - \left(\dot{Y} + d_{\mathrm{la}}\dot{\psi}\right). \quad 4.25$$

4.5.4 Vehicle positioning

Acquiring accurate position in a real truck is a challenging task. On the one hand, GPS information would not be useful when the desired accuracy is a few centimetres. On the other hand, using built sensors and cameras for this purpose, requires a complicated data processing that may neither result in reliable nor fast pace information in near future. Therefore, it is necessary to estimate the vehicle position based on available information.

Small yaw angle and negligible side slip assumptions during a manoeuvre would provide the possibility to estimate the lateral position based on the yaw rate. The yaw rate signal with a fast update rate is usually available in vehicles, and it is accurate enough to be used in vehicle control. However, to calculate yaw angle and lateral position based on the yaw rate, it is necessary to integrate the yaw rate once and twice, respectively. The higher the number of integration, the bigger the amount of generated error will be. Therefore, it is preferable not to integrate yaw rate more than once, as in yaw angle (ψ) PD control (in Equation 4.17).

4.6 Speed control

Very similar to the reference path generation, a speed profile V_{ref} is generated by the path planning procedure. The difference between the actual velocity of the vehicle and the reference velocity is defined as the velocity error. The speed control is then a proportional feedback controller acting on the velocity error, which determines the amount of braking force that should be applied to the wheels in order to keep the reference speed.

The total braking force is distributed on axles proportional to the static load. The speed control is then defined as:

$$F_{\mathrm{FB}} = -K_{PV}(V_{\mathrm{ref}} - V) \quad 4.26$$

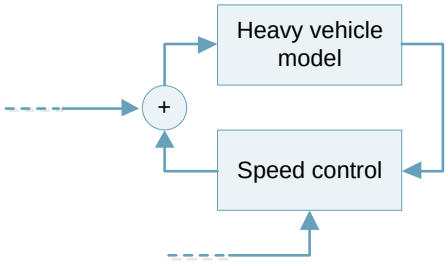

Figure 4.6 Schematic sketch of speed controller.

4.7 Direct yaw moment control

Differential braking is used for direct yaw moment control (DYC). It is used as a feedback control on yaw rate error to control the vehicle yaw motion. The controller uses yaw rate error to determine feedback braking force on each individual wheel on one side of the truck. To calculate the required feedback braking force Equation 4.27 is used.

$$F_{x,i,j}^{\mathrm{FB}} = -K_{PS}\dot{e}_{\psi}\eta_i H_j\left(\dot{e}_{\psi}\right), \quad i = 1{,}2 \quad , \quad j = 1{,}2 \quad 4.27$$

where K_{PS} is the controller gain that if multiplied with yaw rate error, $\dot{e}_\psi$, forms the total yaw moment. η_i is the contribution of i^{th} axle and will be given as a tuning parameter in corresponding simulation part, and $H_j(\dot{e}_\psi)$ is the contribution of the left or right tyre on the axle. $j = 1$ for the left tyre and $j = 2$ for the right one. For DYC, the braking force will only be applied to tyres on the first and the second axle.

$$\sum \eta_i = 1, \quad H_j(\dot{e}_\psi) = \begin{cases} H(\dot{e}_\psi), & j = 1 \\ H(-\dot{e}_\psi), & j = 2 \end{cases}, \tag{4.28}$$

where H is a Heaviside function as

$$H(x) = \begin{cases} 1, & x \geq 0 \\ 0, & x < 0 \end{cases}. \tag{4.29}$$

The total braking force is as

$$F_{x,i,j} = F_{x,i,j}^{\text{FF}} + F_{x,i,j}^{\text{FB}} \tag{4.30}$$

Schematic figure of the yaw controller is provided in Figure 4.7.

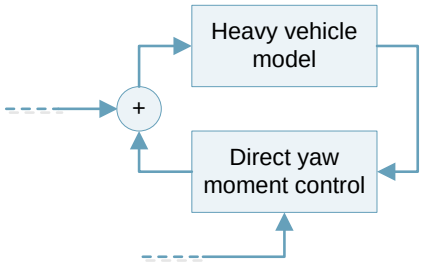

Figure 4.7 Schematic sketch of direct yaw moment controller.

4.8 Complete path and speed control system

In a complete feedback control for collision avoidance application, path and speed control try to avoid an accident by steering and braking while the stability control assures the stability of the vehicle during the manoeuvre. This is represented in a schematic sketch in Figure 4.8.

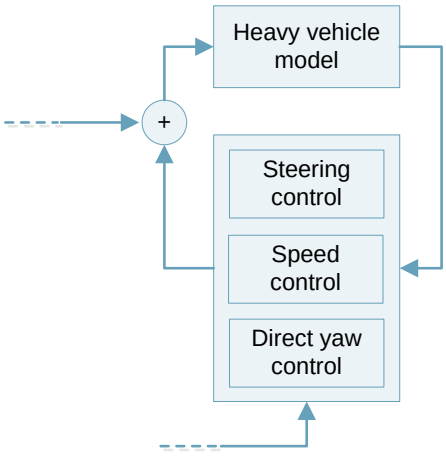

Figure 4.8 Schematic sketch of the complete path and speed control system.

5 Simulation results

The path stability control by steering introduced in Chapter 4 is implemented and applied to the heavy vehicle model introduced in Chapter 2. In order to study the performance of the controller with respect to the availability of the information, simulations are done separately for the lateral position control only and yaw control only, in addition to the complete controller with discrete input information. Simulations are repeated for the all 3 use cases and results are presented in this chapter after the simulation parameter settings are introduced.

5.1 Parameter settings

In addition to the heavy vehicle parameters, there are general path planning parameters and controller settings that are the same for simulation of the all use cases, whereas there are simulation settings specific to each use case, that are mentioned for each use case separately. Heavy vehicle parameters can be found in Table of notations, whereas other parameters are introduced here as follow.

The values used for the constraints in path planning that are imposed by the heavy vehicle manoeuvrability limits and the steering actuator performance, are presented below in Table 5.1.

Constraint	Value
Lateral acceleration, $\lvert a_{y,\max} \rvert$	$3\ \mathrm{m/s^2}$
Steering wheel angle, $\lvert \delta_{\max} \rvert$	$800\ \mathrm{deg}$
Steering wheel angle rate, $\lvert \dot{\delta}_{\max} \rvert$	$430\ \mathrm{deg/s}$
Torque on the steering actuator, $\lvert T_{\max} \rvert$	$25\ \mathrm{Nm}$

Table 5.1 Constraint for the critical path in path planning.

In a collision avoidance application, information from different sources may be available on different update rates and accuracy levels. Although yaw rate information can be reached on a sufficiently high update rate, there are challenges to acquire lateral position information with high update rate. Therefore, the simulations are planned to study performance of the controller for different possible conditions. In the first set of simulations, only the lateral position controller is studied, and it is assumed that lateral information is available with high update rate and without noise, thus the yaw controller gains are set to zero in order to study the later position control standalone. In the second set of simulations, controller is only using the yaw information with high update rate, and gains of the lateral position control are set to zero. Results from the two simulations are plotted beside each other, and can be compared.

Finally, in order to study the limitations of the controller, discrete information is used for the complete controller with certain controller gains, where both lateral position control and yaw control are active while they receive information with different update rates. The update rate is assumed to be $10\ \mathrm{Hz}$ for the lateral position information, and $100\ \mathrm{Hz}$ for the yaw rate information. It is also assumed that the controller demand can be provided with the rate of $100\ \mathrm{Hz}$. Corresponding gains in each simulation set are given in Table 5.2. It is necessary to mention that the controller gains are the same for all use cases. The aim has been to design a robust controller that works for all use cases rather than tuning the controller gains to get the best result for each use case separately. Therefore controller gains that are shown in Table 5.2 are used for simulation of all use cases.

Gain	Lateral position control	Yaw control	Complete controller
K_{PY} [rad/m]	20	0	20
K_{IY} [rad/ m. s]	100	0	0
K_{DY} [s. rad/m]	5	0	5
$K_{P\psi}$ [−]	0	40	0
$K_{D\psi}$ [s]	0	5	2

Table 5.2 Controller gains for simulation of the all use cases.

5.2 RECA

Each use case can be interpreted as specific setting in the simulation. RECA manoeuvre in this simulation includes a single lane change with specific simulation settings as presented in Table 5.3. Note that the simulation is done for high-μ surfaces.

Parameters	Values
Friction, μ	0.65
Lateral distance, b [m]	3
Host vehicle initial velocity, V_H [km/h]	80
Lead vehicle initial velocity,V_L [km/h]	0
Longitudinal distance, d [m]	54
Lookahead time, t_{la} [s]	0.25
Intervention start point, X_{is} [m]	5
Safety margin, η [%]	0

Table 5.3 Specific simulation settings for RECA manoeuvre.

The vehicle position, heading angle, and heading angle rate for the simulation of RECA manoeuvre can be observed in Figure 5.1. Results are presented and can be compared for two controllers; one based on the actual lateral position error, and the other based on the yaw angle error.

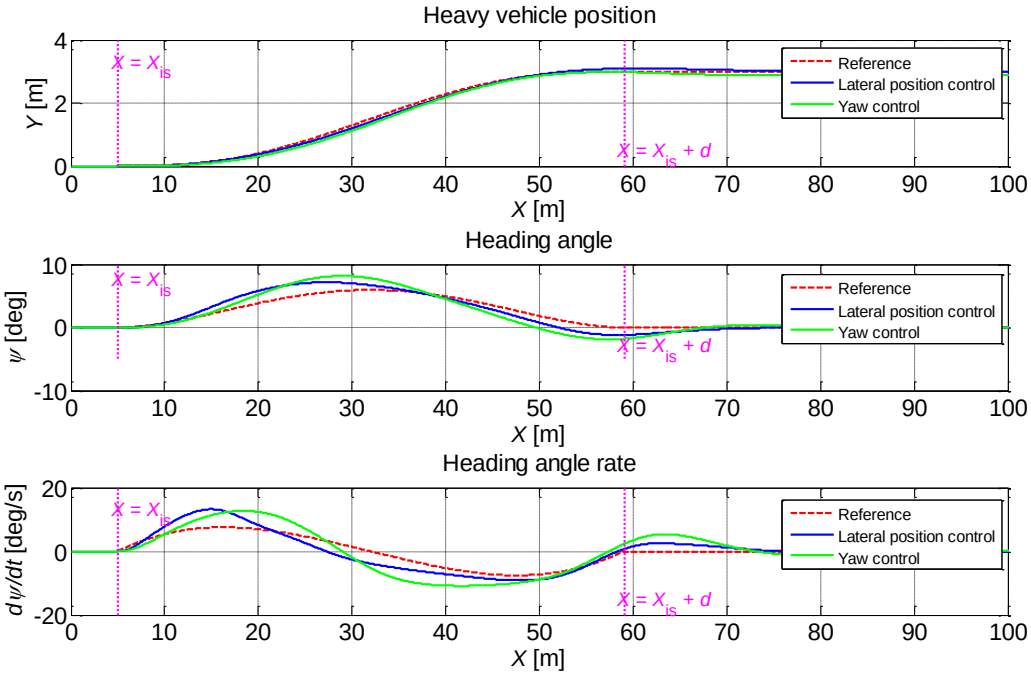

Figure 5.1 Path control results for RECA; position, heading angle, and its rate.

Steering wheel angle and lateral acceleration variations and also their rates can be seen in Figure 5.2. As expected, counter steering is observed in the presence of the feedback control.

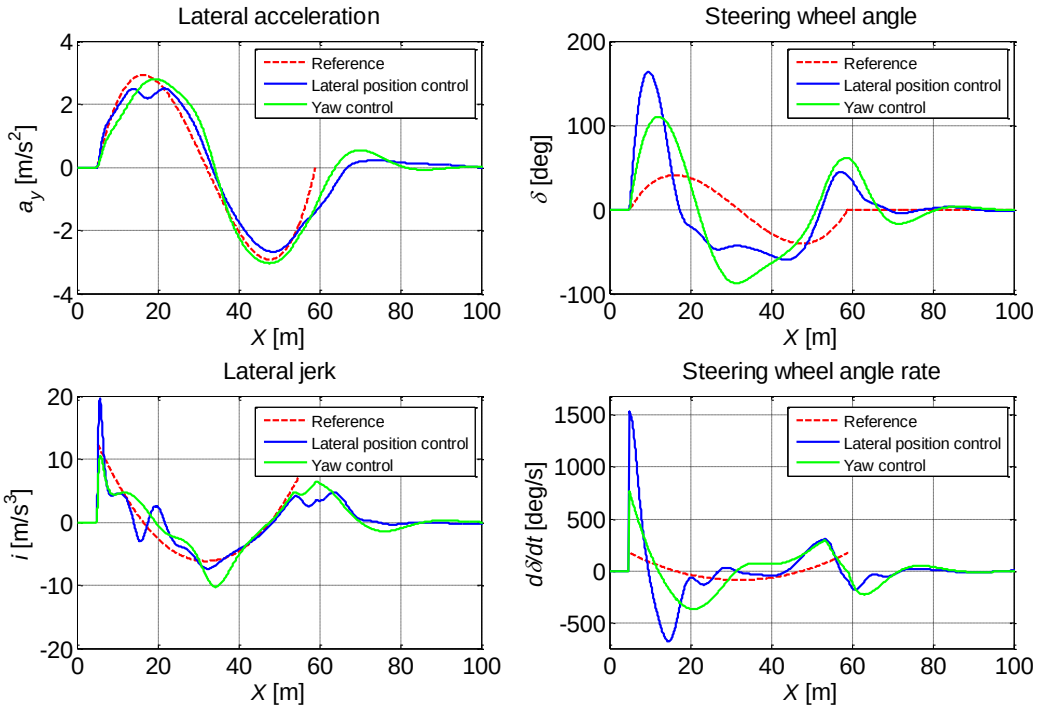

Figure 5.2 Path control results for RECA; lateral acceleration and steering wheel angle, and their rates.

The fifth order polynomial reference path turns out to be suitable to generate continuous profiles for reference steering angle input and lateral acceleration, as shown in Figure 5.2. However, lateral jerk and steering wheel angle rate profiles are not continuous. Although this

may be filtered by either the steering actuator or the heavy vehicle dynamics, it can be counted as a limitation of using the fifth order polynomial. It is possible that, instead, a multiple lower order polynomial would be used in real time collision avoidance application. The order of the polynomial depends on the dynamics, *e.g.* filtering, of the heavy vehicle and the actuators. The framework used here is quite flexible that can easily be replaced and used.

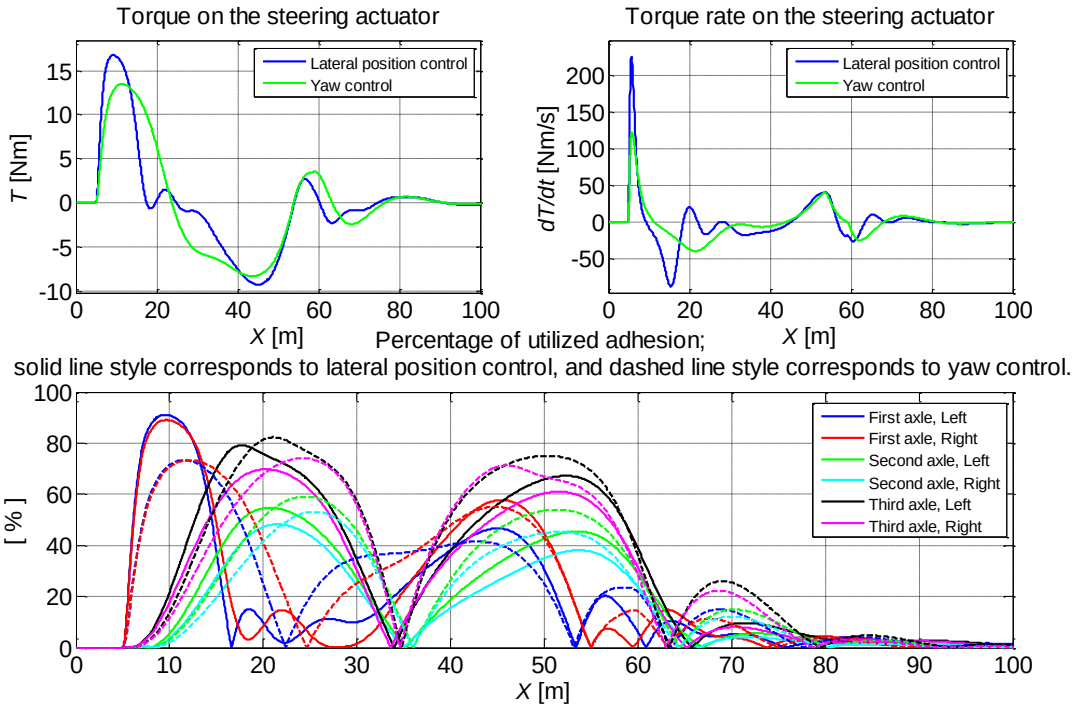

Figure 5.3 Path control results for RECA; torque and utilised tyre capacity.

Steering actuator torque variations, and forces on tyres can be observed in Figure 5.3. As can be seen, the controller based on the lateral position error utilizes more capacity of the tyres, and as a result, makes the heavy vehicle to respond quicker and follow the reference path better. Table 5.4 shows a posteriori performance evaluations result of the simulation. Maximum value for each parameter, the target value and the value of the parameter at the end of the required longitudinal distance, where $X = X_{\mathrm{is}} + d$, are mentioned bellow.

	Max	**Target**	**@$X = X_{\mathrm{is}} + d$**
Lateral position error, e_Y [m]	0.10	0.10	0.10
Yaw angle error, e_ψ [deg]	2.00	1	1.19
Steering angle, δ [deg]	163.17	800	40.20
Steering angle rate, $\dot{\delta}$ [deg/s]	1528.39	430	87.10
Lateral acceleration, a_y [m/s^2]	2.68	3	1.42
Lateral jerk, i [m/s^3]	19.56	5	3.41
Torque on steering actuator, T [Nm]	16.77	25	1.29
Torque rate on steering actuator, $\dot{T}$ [Nm/s]	224.88	100	18.10

Table 5.4 Path control results for RECA with the controller based on the lateral position.

Errors of the two controllers are also compared to each other in Figure 5.4. As expected, the controller based on the lateral position error has a much better performance in general.

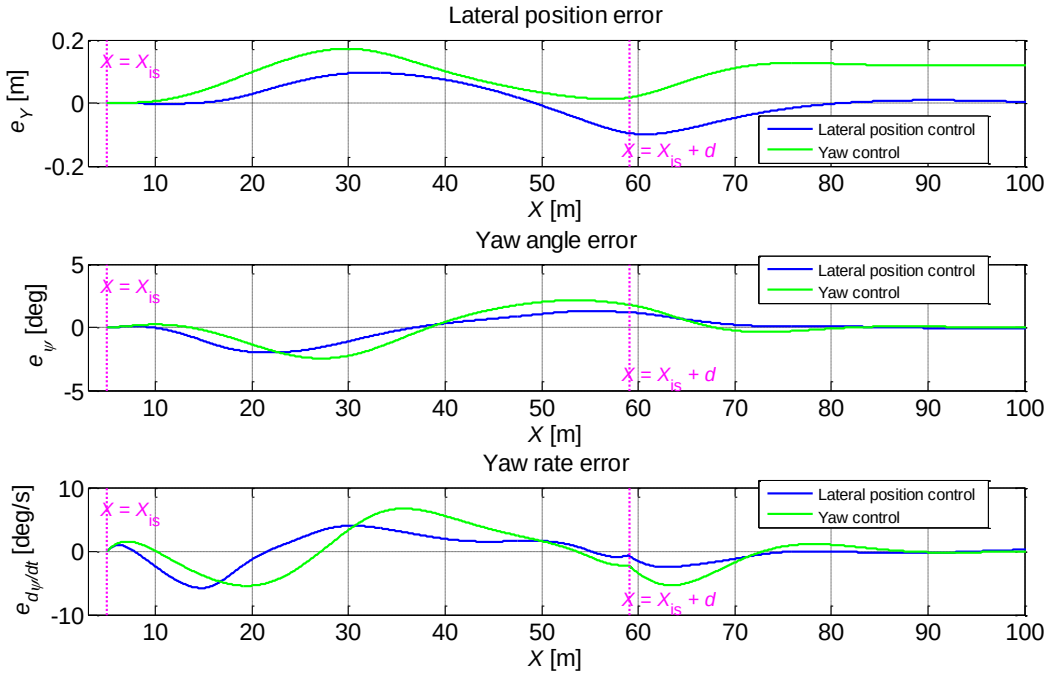

Figure 5.4 Path control results for RECA; error dynamics for two path control algorithms.

The first step is also taken towards matching the simulation environment with the real world experiment situation. The update rate of the information like lateral position is much slower in reality than in simulation. Thus the simulation is repeated for the complete controller based on the discrete lateral position and yaw rate information in contrary to continuously available position information. This may emulate slow update rate of the lateral position signal in a real truck, and also limited update rate of the yaw rate information. In order to emulate limited operating frequency of the steering actuator, the steering command is also discretized with an update rate of 100 Hz. The resulting errors can be observed in Figure 5.5. In order to compensate for the delay due to the slow update rate of the lateral position information, Riemann sum of the estimated lateral position velocity is used between every two consequent update time to estimate the lateral position, when there is no new measured information about lateral position available. The lateral velocity itself is estimated based on longitudinal velocity of the vehicle and the heading angle, as

$$\dot{\hat{Y}} = v_x \sin\psi \qquad 5.1$$

where v_x is the longitudinal speed of the vehicle, and ψ is the yaw angle, and both are measured information with update rate of 100 Hz.

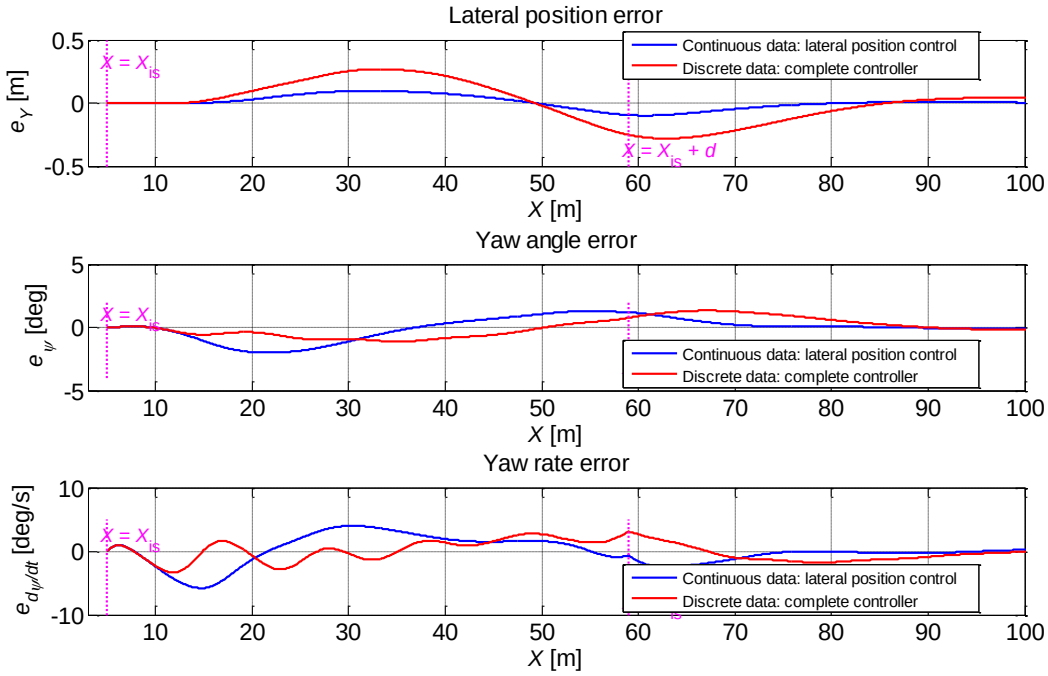

Figure 5.5 Path control results for RECA; error dynamics under the influence of discretized lateral position information.

As can be seen in Figure 5.5, the controller performance when it uses continuous data is obviously better, whereas using discrete information adds some error and oscillations. However, the result is promising when complete controller is used that employs information with both slow and fast update rate.

5.3 RORP on a straight road

The simulation steps taken for RECA are repeated in this section for RORP on a straight road use case. Recalling the description of the use case from Section 1.2.2, the vehicle is assumed to receive false steering input from unattended driver thus running off the road. The controller, if activated, is supposed to start the intervention when the deviation of the vehicle from the centre of the lane, b_{d}, reaches a certain limit, and take the vehicle back to the centre of the lane by performing a suitable manoeuvre.

Same as RECA use case, there are specific settings for RORP on a straight road. Table 5.5 shows the specific simulation settings that can be interpreted from definition of the use case. Note that only the steering control is used in this simulation.

Parameters	Values
Friction, μ [−]	0.65
Host vehicle initial velocity, V_H [km/h]	65
Longitudinal distance, d [m]	31
Lookahead time, t_{la} [s]	0.25
Run-off limit, b_{d} [m]	0.2
Driver's false steering input, δ_{d} [deg]	40
Intervention start point, X_{is} [m]	19.26
Safety margin, η [%]	0

Table 5.5 Specific simulation settings for RORP on a straight road.

Other parameter values are described in Sections 5.1, and can be found in Table 5.1, Table 5.2, and Table of notations.

Vehicle position, heading angle, and its rate are observable in Figure 5.6, whereas the lateral acceleration and the steering wheel angle and also their rates are presented in Figure 5.7. Similar to the results for RECA, the controller based on the lateral position respond faster to the steering input.

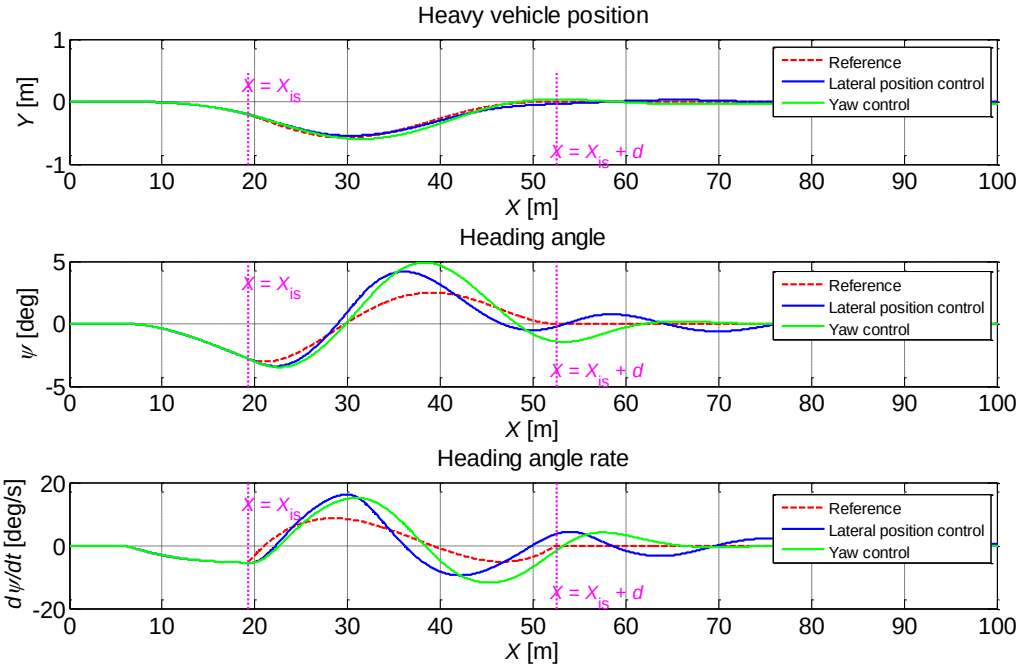

Figure 5.6 Path control results for RORP on a straight road; position, heading angle, and heading angle rate.

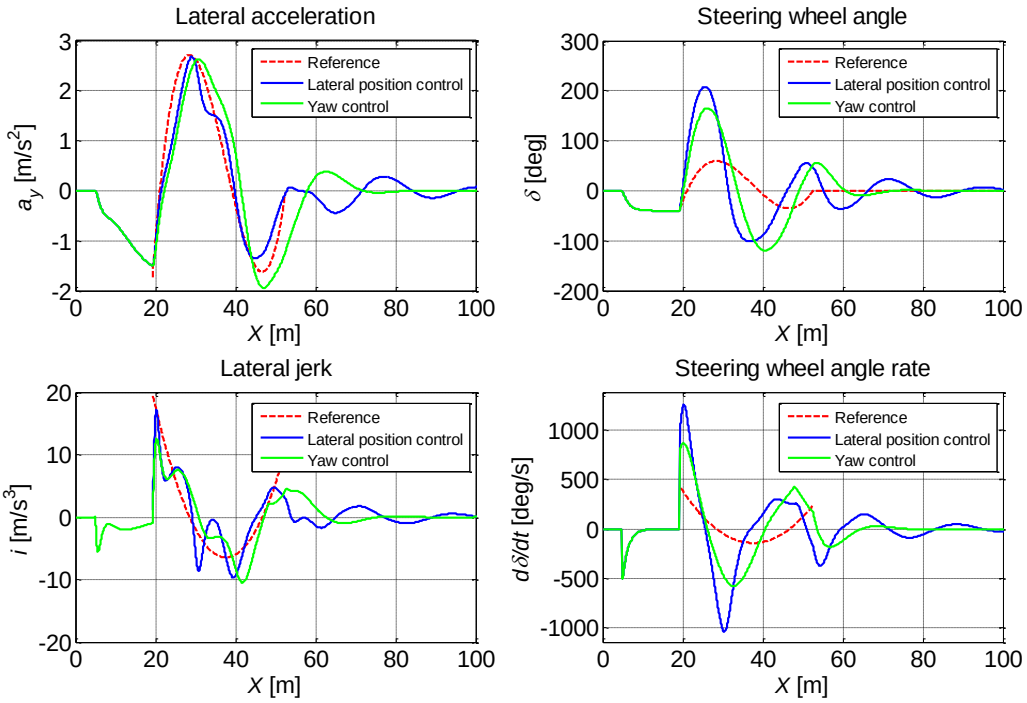

Figure 5.7 Path control results for RORP on a straight road; lateral acceleration, steering angle, and their rate.

Similar to RECA, the discontinuity of the lateral jerk and steering angle rate is also present in RORP on a straight road, as shown in Figure 5.7. It is also worth to notice that the continuity of the reference steering angle and lateral acceleration profiles are dependent on the accuracy of the information about heading angle at the start of the intervention.

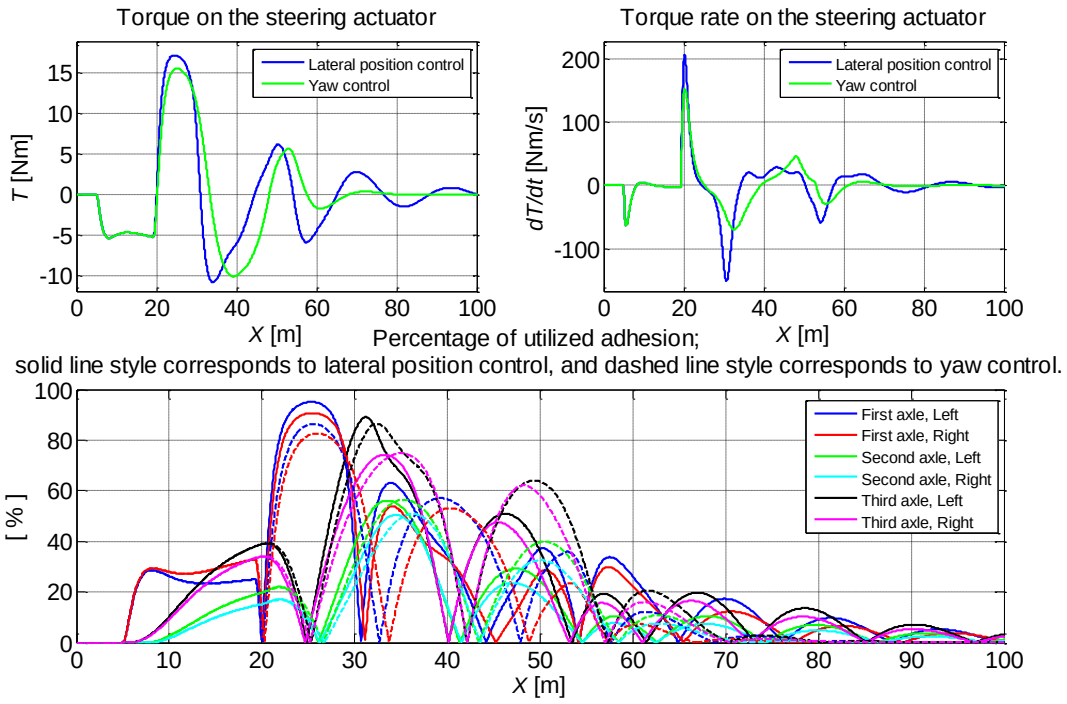

Figure 5.8 Path control results for RORP on a straight road; torque and utilised tyre capacity.

Table 5.6 shows a posteriori performance evaluations result of the simulation. Maximum value for each parameter, the target value and the value of the parameter at the end of the required longitudinal distance, where $X = X_{\text{is}} + d$, are mentioned bellow. The high and unacceptable values of the steering angle rate and wheel torque rate shall be investigated more, although they will be filtered by the actuator dynamics in a heavy vehicle.

	Max	**Target**	**@$X = X_{\text{is}} + d$**
Lateral position error, e_Y [m]	0.20	0.10	0.04
Yaw angle error, e_ψ [deg]	2.11	1	0.23
Steering angle, δ [deg]	207.96	800	47.41
Steering angle rate, $\dot{\delta}$ [deg/s]	1258.01	430	161.19
Lateral acceleration, a_y [m/s^2]	2.68	3	0.04
Lateral jerk, i [m/s^3]	17.21	5	2.92
Torque on steering actuator, T [Nm]	17.17	25	4.15
Torque rate on steering actuator, $\dot{T}$ [Nm/s]	206.63	100	30.45

Table 5.6 Path control results for RORP on a straight road with controller based on the lateral position error.

Errors of the two controllers are also compared to each other in Figure 5.9. As expected and similar to the RECA use case, the controller based on the lateral position error has a much better performance in general.

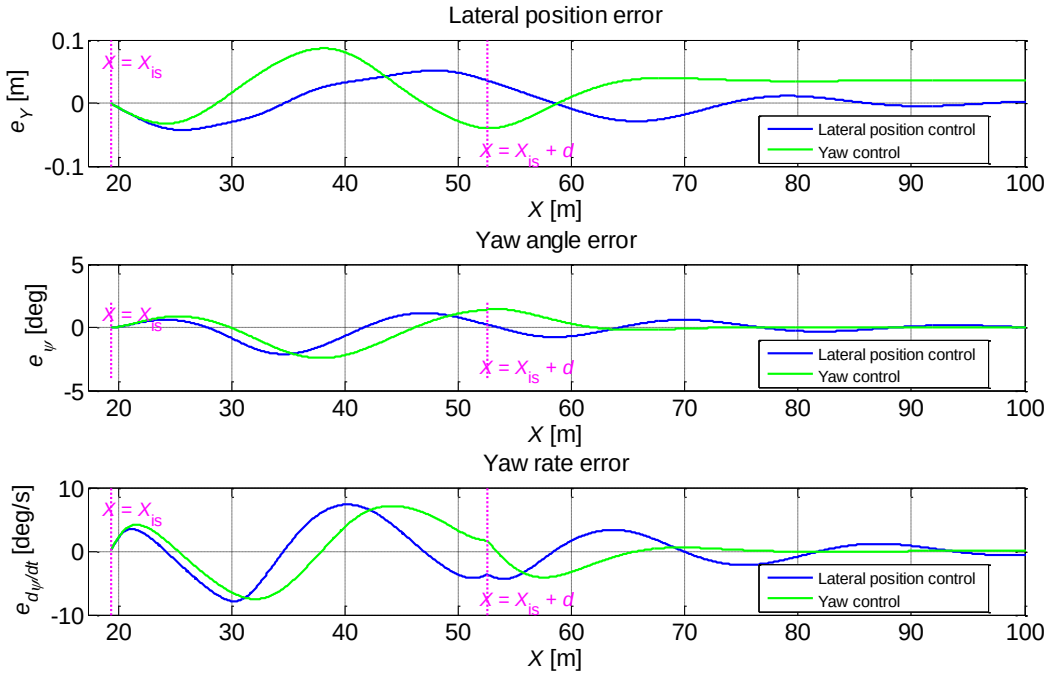

Figure 5.9 Path control results for RORP on a straight road; error dynamics for two path control algorithms.

Similar to RECA use case, the first step is also taken towards matching the simulation environment with the real world experiment situation. The update rate of the information like lateral position is much slower in reality than in simulation. Thus the simulation is repeated for the complete controller based on the discrete lateral position and yaw rate information in contrary to continuously available position information. This may emulate slow update rate of the lateral position signal in a real truck, and also limited update rate of the yaw rate information. In order to emulate limited operating frequency of the steering actuator, the steering command is also discretized with an update rate of 100 Hz. The resulting errors can be observed in Figure 5.10. In order to compensate for the delay due to the slow update rate of the lateral position information, Riemann sum of the estimated lateral position velocity is used between every two consequent update time to estimate the lateral position, when there is no new information about lateral position available. The lateral velocity itself is estimated based on the longitudinal velocity of the vehicle and the heading angle as in Equation 5.1.

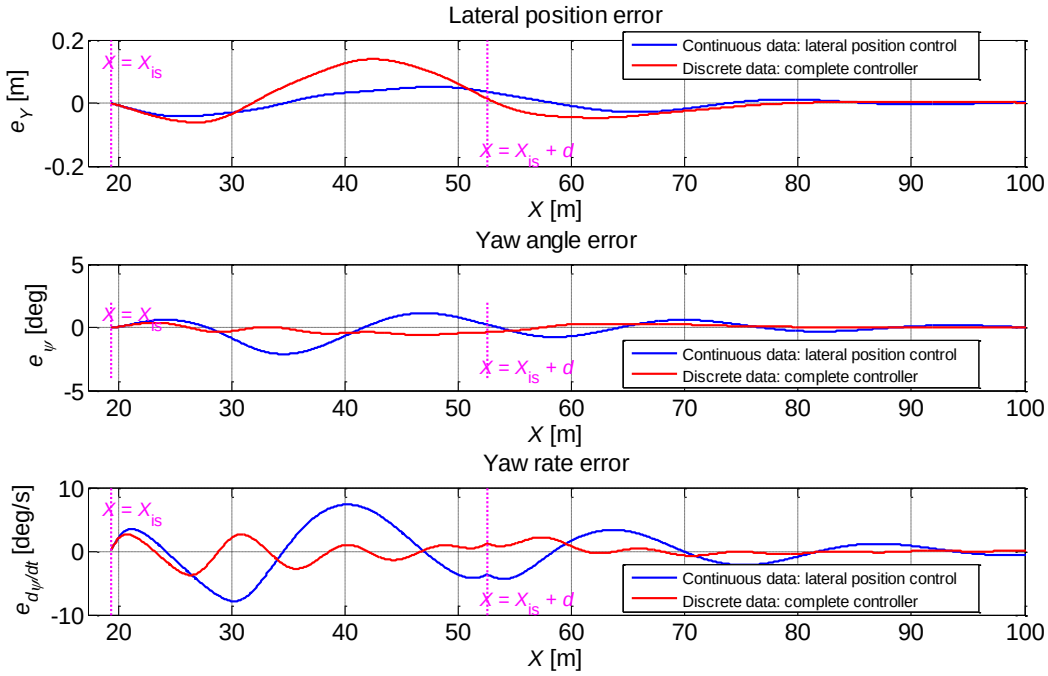

Figure 5.10 Path control results for RORP on a straight road; Error dynamics under the influence of discretized lateral position information.

As can be seen in Figure 5.10, the controller performance when it uses continuous data is obviously better, whereas using discrete information adds some error and oscillations. However, the result is promising when complete controller is used that employs information with both slow and fast update rate.

5.4 RORP in a curve

Recalling the description of this use case, the vehicle is running off the curve due to lack of suitable steering input by driver. Therefore the controller should start intervention and bring the vehicle back in the curve when the distance between CG and centre of the road reaches a certain limit, b_{L}. The steps taken in simulations for this use case is also same as the other two as described in the last two chapters.

Table 5.7 shows the specific simulation settings that can be interpreted from definition of this use case; RORP in a curve. Note that only the steering control is used in this simulation, and the simulation is done on high-μ surface.

Parameters	Values
Friction, μ $[-]$	0.65
Host vehicle initial velocity, V_H $[\mathrm{km/h}]$	65
Required longitudinal distance, d $[m]$	73
Lookahead time, t_{la} $[\mathrm{s}]$	0.25
Run-off limit, b_{d} $[\mathrm{m}]$	0.2
Radius of the road curvature, R_{r} $[\mathrm{m}]$	200
Intervention start point, X_{is} $[\mathrm{m}]$	14
Safety margin, η $[\%]$	0

Table 5.7 RORP in a curve parameter setting.

Other parameter values are described in Sections 5.1, and can be found in Table 5.1, Table 5.2, and Table of notations.

Vehicle position, heading angle, and its rate are observable in Figure 5.11, whereas lateral acceleration and steering wheel angle and also their rates are presented in Figure 5.12. Similar to the results for RECA, the controller based on the lateral position respond faster to the steering input.

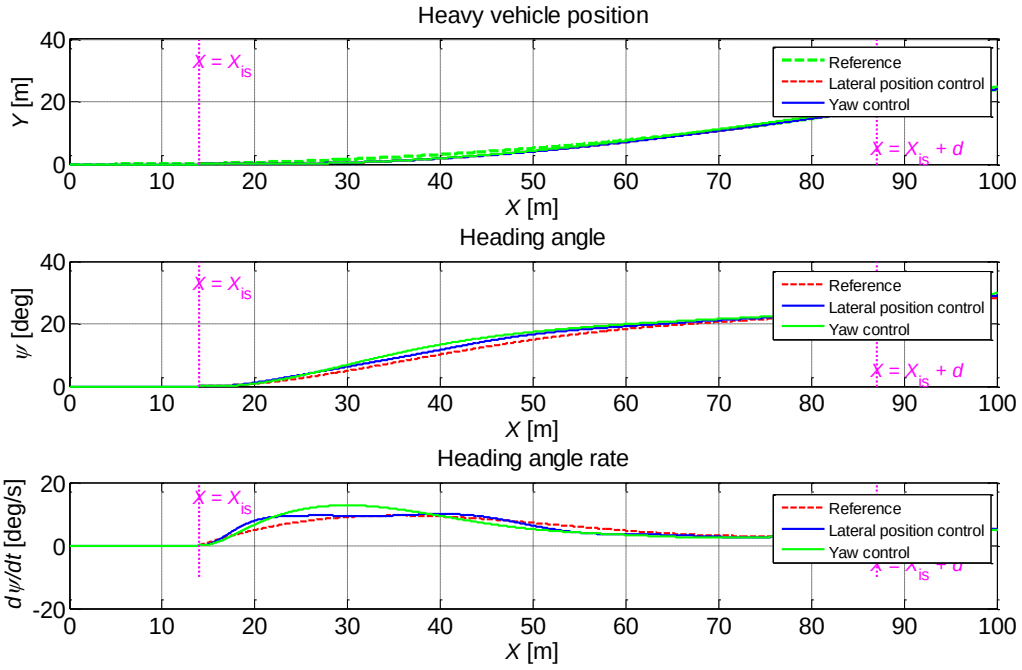

Figure 5.11 Path control results for RORP in a curve; position, heading angle, and its rate.

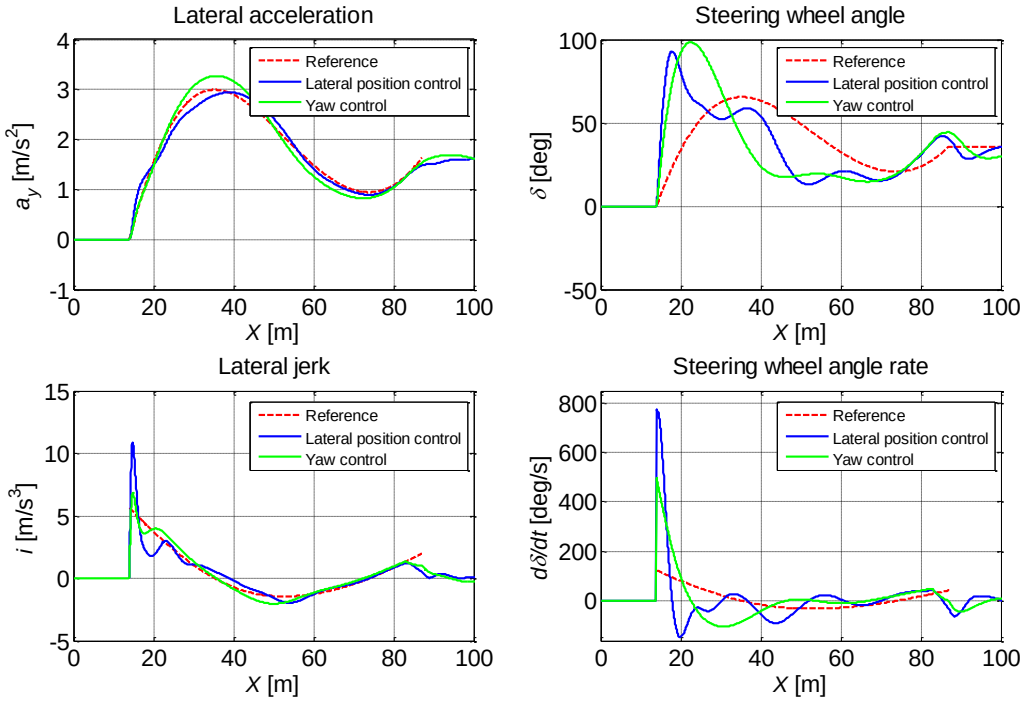

Figure 5.12 Path control results for RORP in a curve; lateral acceleration, steering angle, and their rate.

Similar to the previous use cases, the discontinuity of the lateral jerk and steering angle rate is also present in RORP in a curve, as shown in Figure 5.12. It is also worth to notice that the continuity of the reference steering angle and lateral acceleration profiles are dependent on the accuracy of the information about heading angle at the start of the intervention.

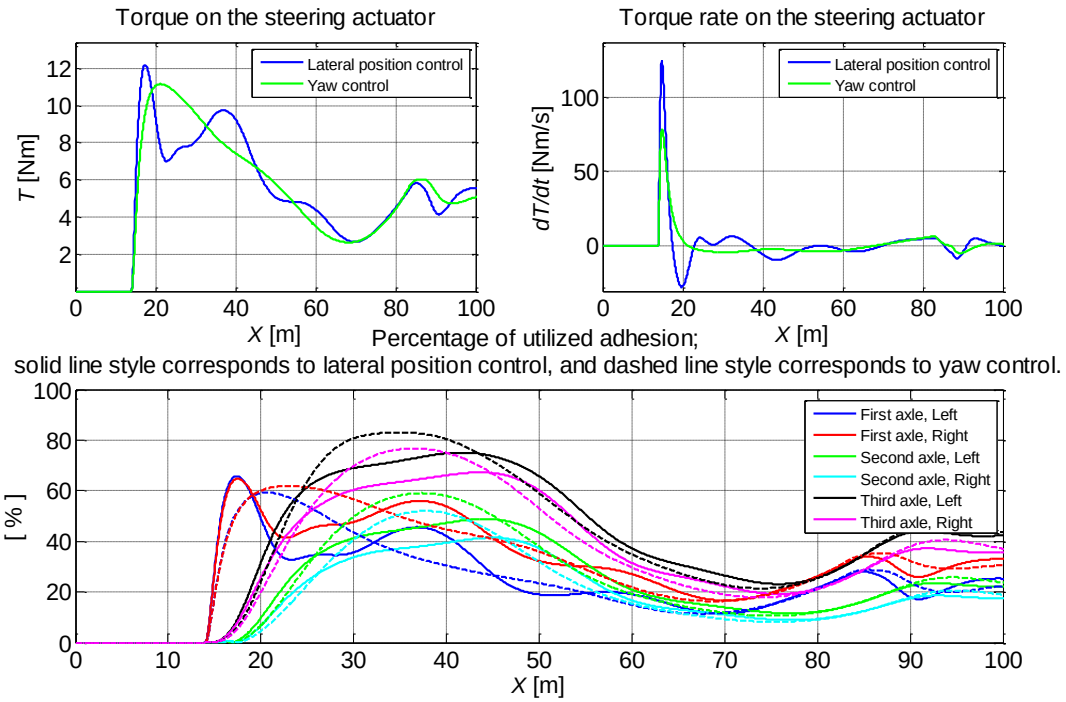

Figure 5.13 Path control results for RORP in a curve; torque and utilised tyre capacity.

Table 5.8 shows a posteriori performance evaluations result of the simulation. Maximum value for each parameter, the target value and the value of the parameter at the end of the required longitudinal distance, where $X = X_{\mathrm{is}} + d$, are mentioned in Table 5.8.

	Max	**Target**	**@$X = X_{\mathrm{is}} + d$**
Lateral position error, e_Y [m]	0.06	0.10	0.01
Yaw angle error, e_ψ [deg]	1.80	1	0.59
Steering angle, δ [deg]	92.70	800	40.64
Steering angle rate, $\dot{\delta}$ [deg/s]	771.06	430	30.19
Lateral acceleration, a_y [m/s^2]	2.94	3	1.48
Lateral jerk, i [m/s^3]	10.85	5	0.56
Torque on steering actuator, T [Nm]	12.18	25	5.56
Torque rate on steering actuator, $\dot{T}$ [Nm/s]	124.75	100	4.52

Table 5.8 Path control results for RORP in a curve with the controller based on the lateral position.

Errors of the two controllers are also compared to each other in Figure 5.14. As expected and similar to RECA use case, the controller based on the lateral position error has a much better performance in general.

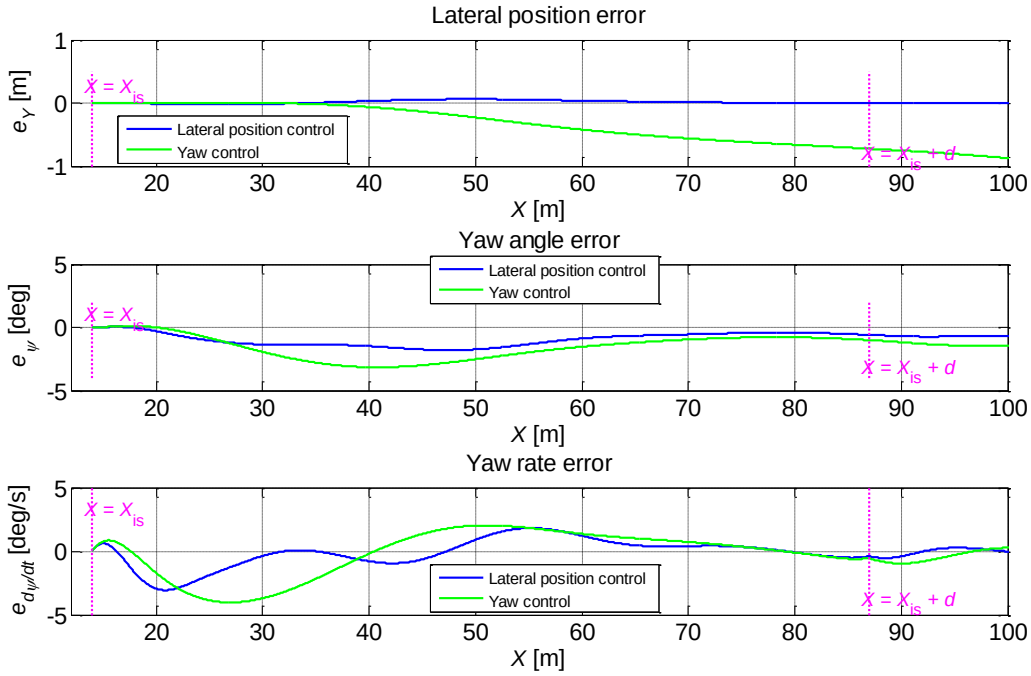

Figure 5.14 Path control results for RORP in a curve; error dynamics for two path control algorithms.

Similar to the previous use case, the first step is also taken towards matching the simulation environment with the real world experiment situation. The update rate of the information like lateral position is much slower in reality than in simulation. Thus the simulation is repeated for the complete controller based on the discrete lateral position and yaw rate information in contrary to continuously available position information. This may emulate slow update rate of the lateral position signal in a real truck, and also limited update rate of the yaw rate information. In order to emulate limited operating frequency of the steering actuator, the steering command is also discretized with an update rate of 100 Hz. The resulting errors can be observed in Figure 5.15. In order to compensate for the delay due to the slow update rate of the lateral position information, Riemann sum of the estimated lateral position velocity is used between every two consequent update time to estimate the lateral position, when there is no new information about lateral position available. The lateral velocity itself is estimated based on the longitudinal velocity of the vehicle and the heading angle as in Equation 5.1.

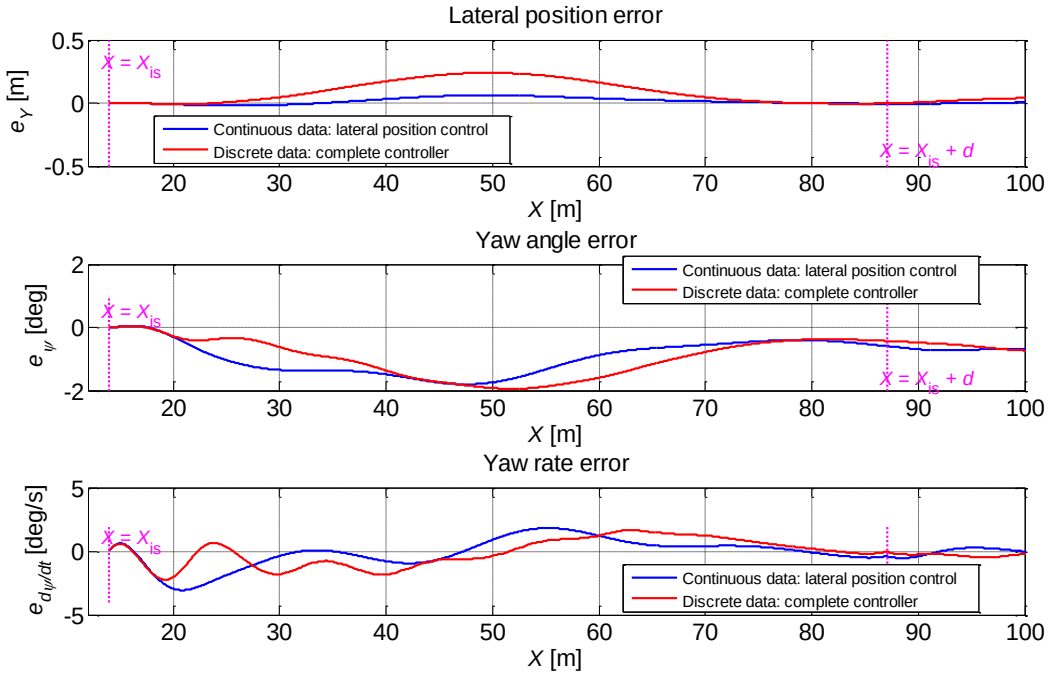

Figure 5.15 Path control results for RORP in a curve; error dynamics under the influence of discretized lateral position information.

As can be seen in Figure 5.15, the controller performance when it uses continuous data is obviously better, whereas using discrete information adds some error and oscillations. However, the result is promising when complete controller is used that employs information with both slow and fast update rate.

6 Experimental results

In order to both test the performance of the controller and empirically verify the model, a very direct way is to conduct a manoeuvre with both simulated and real truck and then compare the results. The closer the test condition would be to the simulation settings, the more successful the comparison will be. In this study, a series of tests were done on sunny Friday of September 28, 2012, in handling area of Volvo test track at Hällered, Sweden. Closed loop control of the truck was done for RECA manoeuvre with sufficient safety margin. Several signals were logged including position of the truck using RTK-GPS reference positioning system installed in the test area. Test condition is described in this chapter following the comparison of the results. Through presented results, it is possible to observe the performance of the current controller in a real experiment, and also to qualitatively validate the simulation model by feeding the logged steering angle of the test data as input to the simulation model.

6.1 The experiment settings

A truck was planned to do a single lane change manoeuvre. Since having control over all test settings and vehicle parameters in order to match them with simulation settings is not trivial, a lot of effort were made to do the test in a way that can be simulated with the same conditions. However, some minor deviations may still remain due to offset or lag in different components of the truck system, which are not included in simulation model. Moreover, some of the vehicle parameters are good approximation of the real value but not the exact value.

The vehicle path controller was loaded on a *MicroAutoBox II,* and controlled the truck during the lane change. It received yaw rate signal as input, and with the help of a steering actuator, implied a steering angle to the truck in order to perform the lane change. The yaw angle value for the feedback controller was calculated by integrating the yaw rate response.

6.2 Comparing simulation results with test data

The steering angle demand of the controller and the response of the steering actuator can be seen in Figure 6.1. All data come from the logged signals. It can be observed that the actuator was good in following the demand of the controller in the first half of the lane change. However, there are some unexpected deviations between the controller demand and the actuator response that may deteriorate the performance of the vehicle path controller.

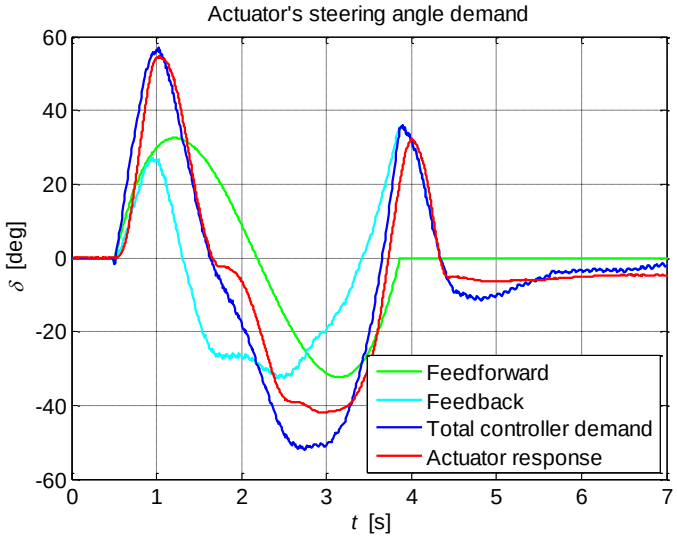

Figure 6.1 Recorded steering input during the lane change.

In order to validate the truck model through a simulation, the logged steering angle during the lane change in the experiment was also used directly as input to the truck model, and the lane change was simulated. Results from simulation are compared here to the corresponding recorded data from the experiment.

Yaw rate is a good indicator in comparison. As can be seen in Figure 6.2 computer simulation is fairly in agreement with the experiment in terms of yaw rate.

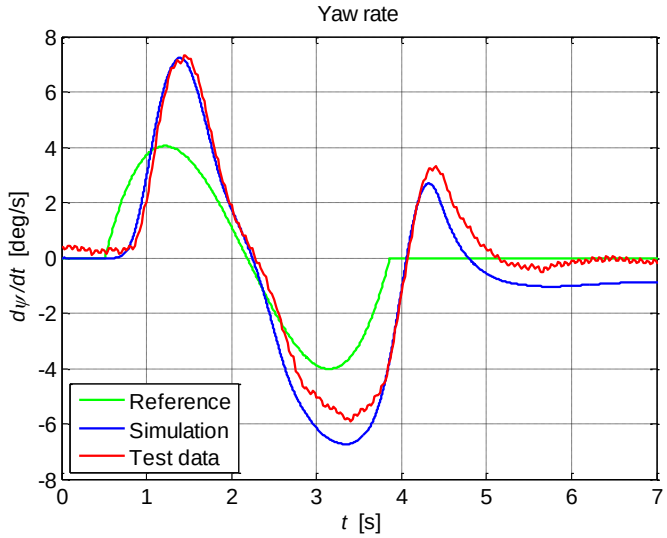

Figure 6.2 Variation of yaw rate during the lane change.

Lateral acceleration is another important measure. As can be seen in Figure 6.3, there is also a good agreement between simulation and test data. Although the general trend is the same in variations of lateral acceleration for both experiment and simulation, the peak value of the lateral acceleration sometimes is not reached in the simulation. This might have roots in simplifications considered in the simulation model, but also in the deviations of the vehicle parameters in simulation environment from real test truck.

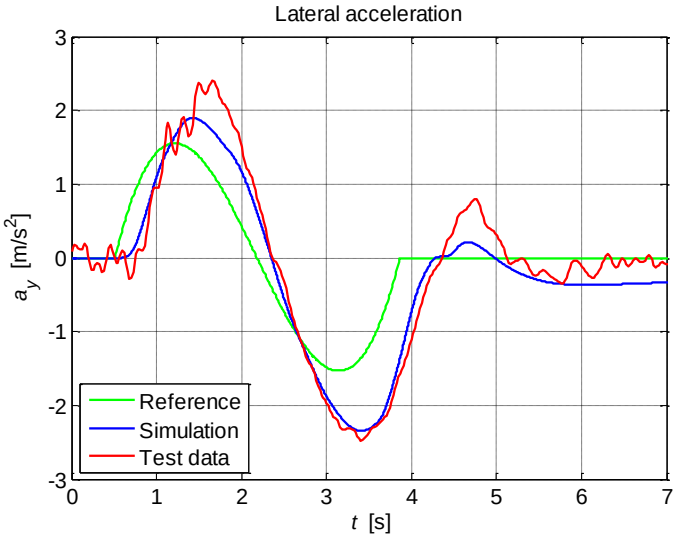

Figure 6.3 Lateral acceleration during the lane change.

Figure 6.4 shows the path during the lane change. A zero steering angle was demanded for a couple of seconds prior to the intervention, in order to keep the truck move on a straight line. Despite the best effort done in this regard, the lateral acceleration and yaw rate are not zero prior to intervention, neither the movement of the truck would be on a perfectly straight line. Therefore, the alignment of the truck trajectory that is done based on the truck movement prior to the intervention, brings some errors to the presented result.

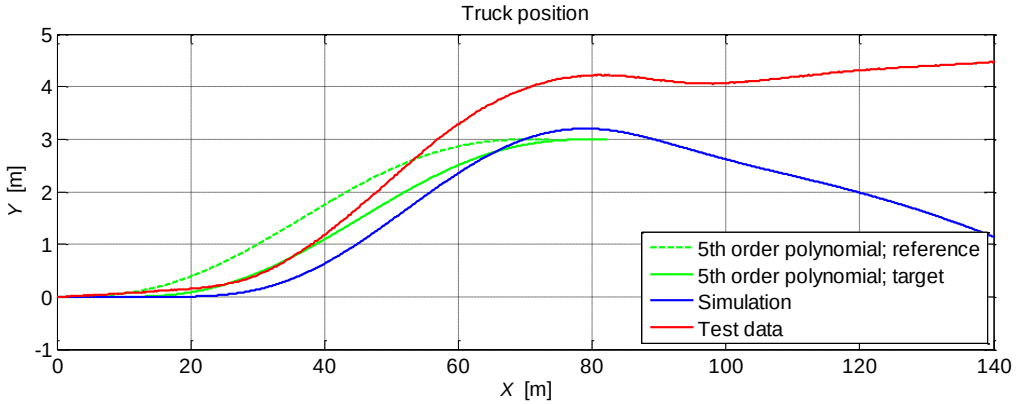

Figure 6.4 Path during the lane change.

In addition, speed of the truck is changing more in the experiment during the lane change than it does in the simulation. This can be observed in Figure 6.5. Variations in the speed also indicates that traction and braking were applied in the experiment while they are not modelled in the simulation. This can be another root for deviations in results.

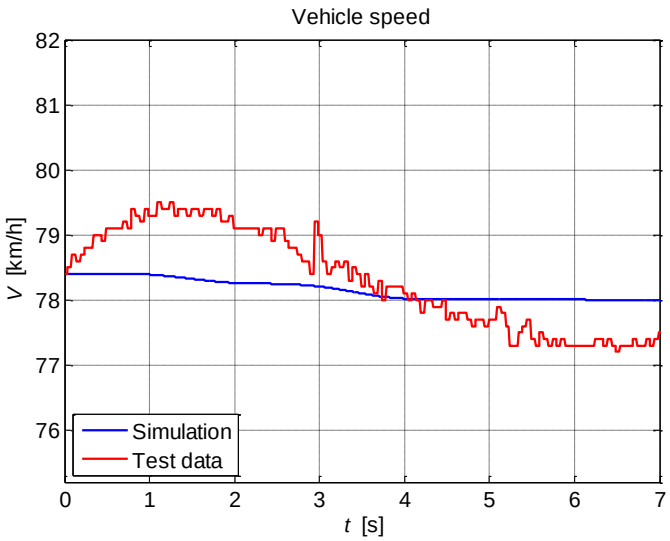

Figure 6.5 Speed variations during the lane change.

7 Simulation and results for passenger cars

7.1 veDYNA simulation environment

veDYNA is a commercial simulation environment for passenger cars. Figure 7.1 shows the animation window of veDYNA.

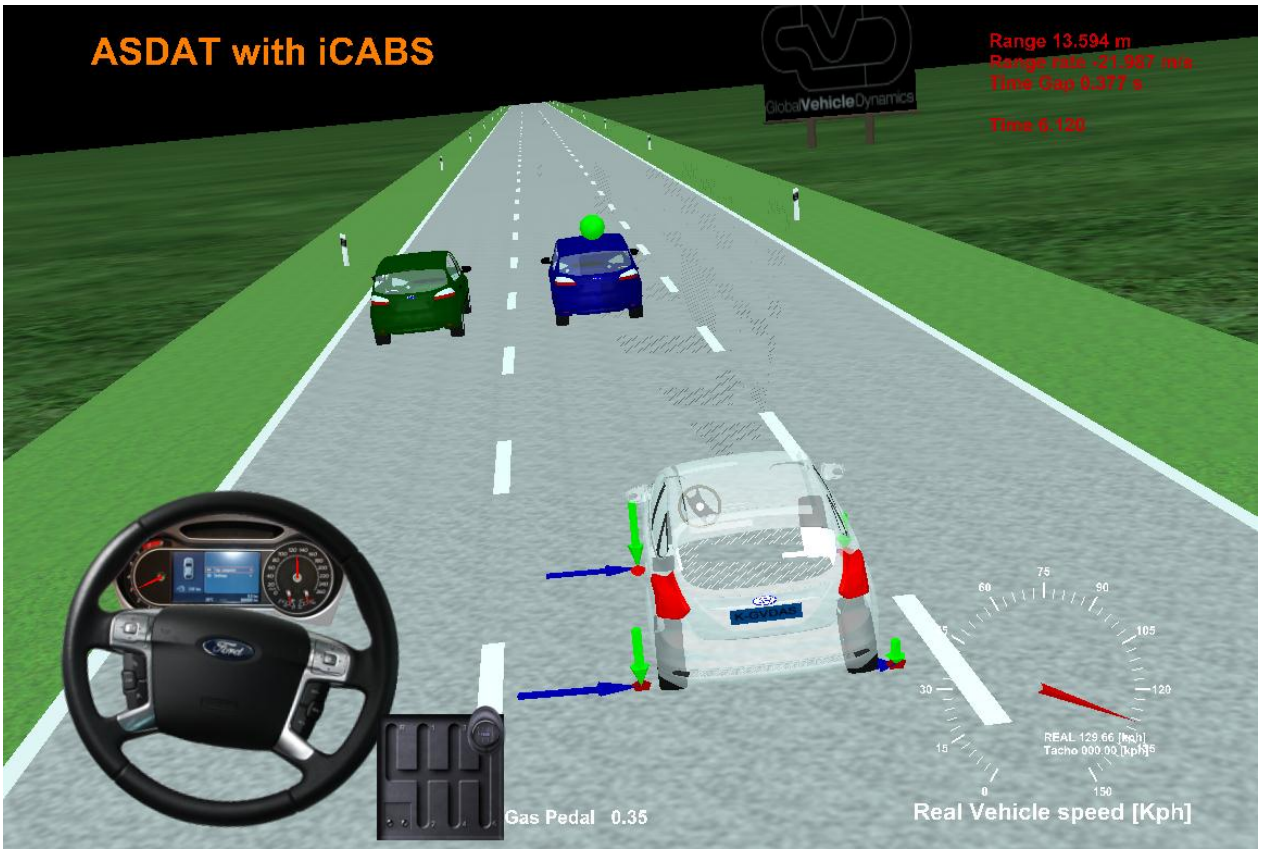

Figure 7.1 Animation window of the veDYNA simulation environment.

veDYNA(**ve**hicle **DYN**amic a**NA**lysis) software is used as software framework and simulation environment for collision avoidance by steering of passenger cars (Figure 7.1 and Figure 7.2). The veDYNA vehicle model is composed of several components such as chassis, engine, driveline and brakes. These main modules are again structured according to their physical and technical constructions. Additionally, veDYNA comes with open and closed loop manoeuvre controllers, driver model and road definition. The new Ford Focus vehicle model is used in this study. The suspension is modelled as kinematic and compliance table. The tyre model is TM-Easy, a semi-empirical model, which yields very realistic results.

The veDYNA modules are coded in C, while data flow and the assembly of the model components are modelled in Simulink. In case of veDYNA Entry, the veDYNA Simulink model is compiled to create a Windows executable, which can be configured via parameters entered in the MATLAB - based Graphical User Interface.

The MATLAB/Simulink environment required for veDYNA Light and veDYNA Standard supports an open structure and allows external and user-defined models to be plugged in easily. Pre-processing, post processing, and the Graphical User Interface of all veDYNA editions is based on MATLAB, therefore a programmable interface is available with full MATLAB functionality.

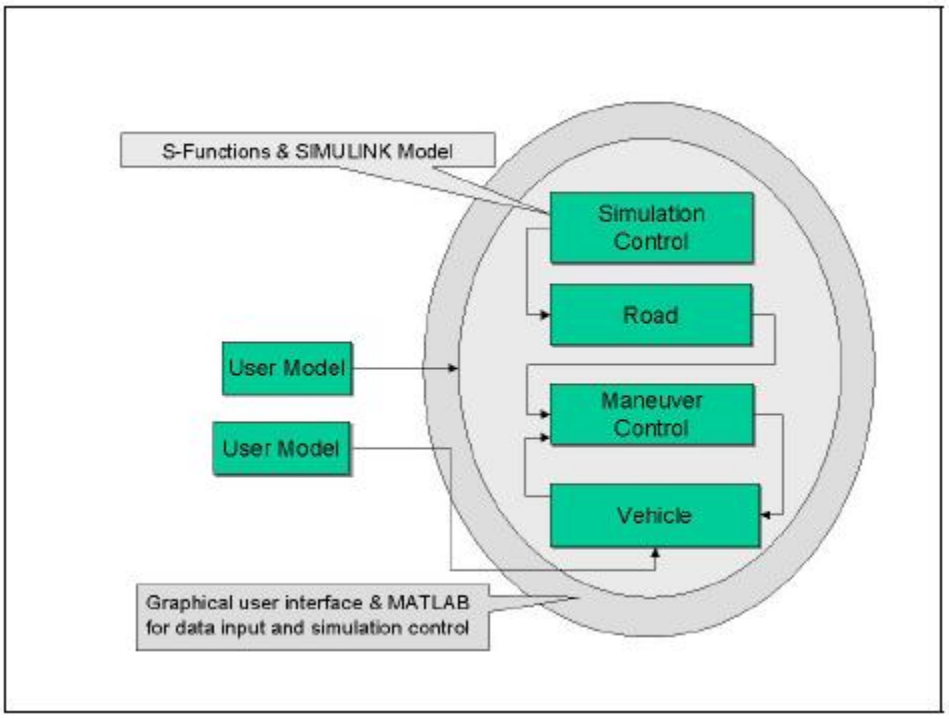

Figure 7.2 Schematic block diagram for veDYNA

7.2 Collision avoidance by steering for passenger cars

This section deals with the development of rear end collision avoidance controller for passenger cars. a single lane change manoeuvre is considered in order to avoid the collision.

ESC system is always on in this simulations, therefore in over-/understeer conditions the ESC system helps to stabilize the vehicle.

7.3 Path control

The control scheme of the lane change is made of state feedback and preview control of the path.

7.3.1 Path planning

Fifth order polynomial is used for defining the escape path for the collision avoidance manoeuvre. The reference signals has been derived from the desired trajectory at desired speed.

7.3.2 Steering control

The feedforward steering angle is generated based on the following equation.

$$\delta_{FF} = \frac{L}{R} + \frac{m}{l}\left(\frac{l_r}{C_f} - \frac{l_f}{C_r}\right)\frac{v^2}{\rho} \qquad 7.1$$

For the feedback loop, the linear PD control is designed for yaw rate and yaw angle.

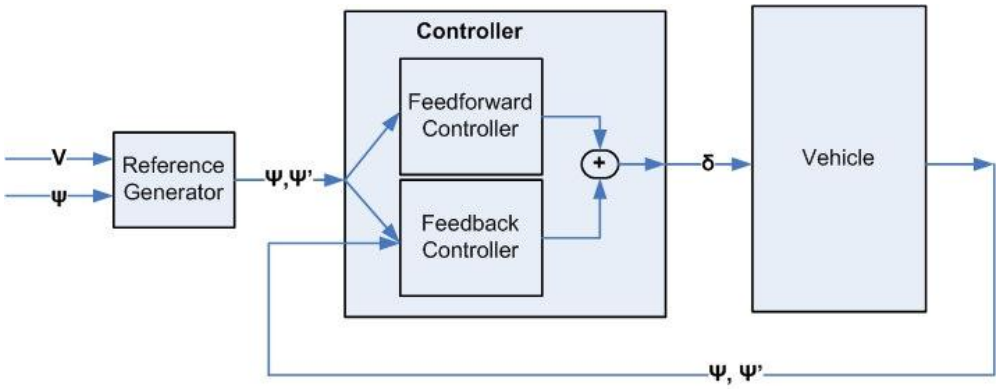

Figure 7.3 Schematic sketch of the controller.

7.4 Simulation

The controller defined in section 7.3 is implemented on the vehicle to investigate the performance the controller.

7.4.1 Test condition

Vehicle velocity : 100 kph
Requested lateral distance : 3 m
Friction: 1.0

7.4.2 Vehicle parameters

Mass = 1528 kg
Moment of Inertia = 2346 kgm2
C.G behind the front bumper; = 1.157 m
Cornering Stiffness = 85247 N/rad
ALC.Var.Cr = 122517 N/rad
Wheelbase = 2.84 m

7.4.3 Simulation results

The results of the path control simulation in a single lane change manoeuvre is as follow:

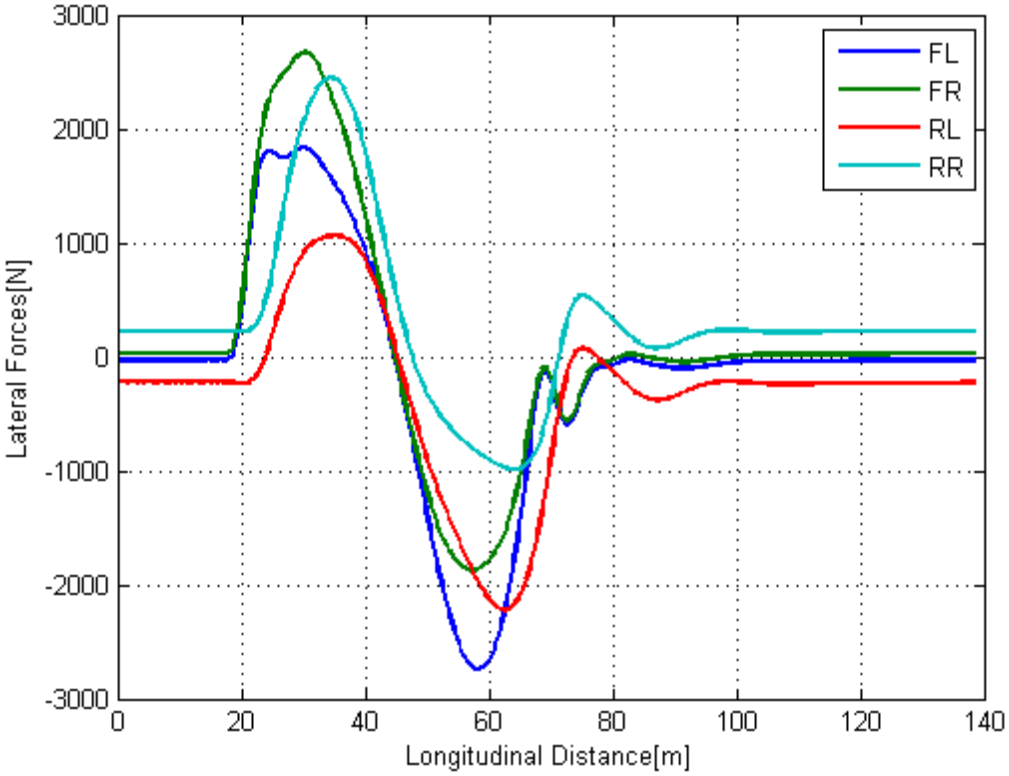

Figure 7.4 Lateral forces versus longitudinal distance.

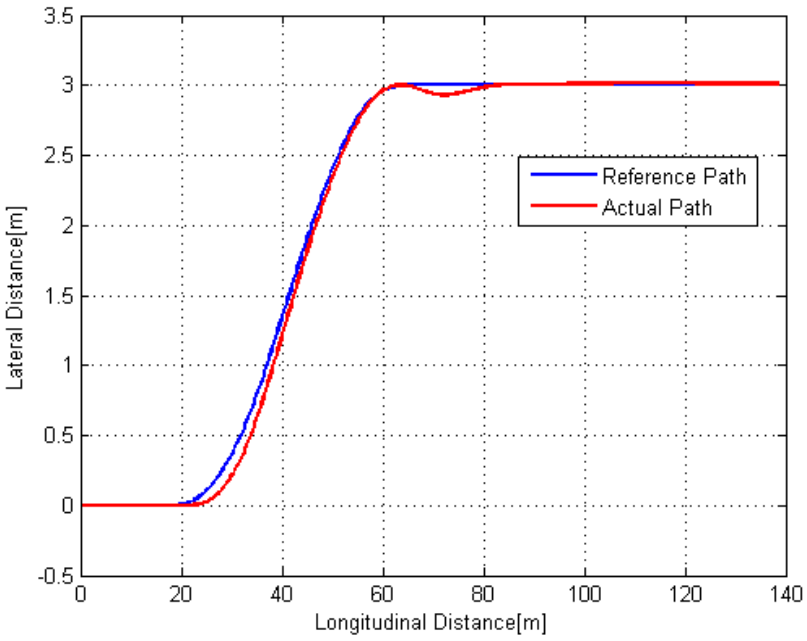

Figure 7.5 Reference and actual position of the vehicle.

8 Conclusions and future work

8.1 Conclusions

A heavy vehicle dynamics model is implemented, and is verified by comparing simulation results to test data and tuning some vehicle parameters. To simulate path control for certain manoeuvres based on the use cases, a path planning procedure is employed, which also provides the feedforward steering input to the vehicle. In addition to the feedforward control, a feedback controller is also employed to compensate for the errors from simplifications and uncertainties. The aim has been to design a robust controller that works for all use cases rather than tuning it for a better performance for each use case separately. Therefore, a simulation tool is developed that can be used for future works and developments. Moreover, results from simulations show that the controller is successful to perform a suitable steering manoeuvre for all use cases with gains that are the same for all of the use cases. If available, the feedback controller performs well based on lateral position information. Otherwise, it can perform the manoeuvre based on available data, including lateral position and yaw rate with different update rates. It can also use yaw rate information only, and since ESC is also using yaw rate, it is possible for the feedback controller to get into interaction with the ESC system. The controller based on heading angle information is also successful in performing the manoeuvre for the passenger car.

When the feedback part is added to the feedforward control, the counter steering appears as expected. Moreover, the peaks of steering angle is more than feedforward steering angle and this is due to the simple model used in the feedforward, which does not take the heavy vehicle yaw dynamics into account. The same happens with the torque on the wheel; therefore more torque is required from steering actuator when the feedback part is added.

8.2 Future work

The fifth order polynomial works well for the path planning. However, using the fifth order polynomial can lead to strange paths if the given manoeuvre deviate a lot from defined use cases. Moreover, there might be other path planning approaches, which may increase the performance by decreasing the required longitudinal distance, improved robustness, and increased controllability. For example, considering actuator filtering may provide an opportunity to use lower order polynomials for path planning.

Currently used set of data for constraint should be updated and completed. Moreover, some robust performance indicators should be defined in order to assist the performance evaluation of the developed path controller.

Although the feedback part of the controller manage to eliminate errors of the system to a reasonable extent, improvements of the feedforward part can help to increase the overall performance of the work and to make the task of the feedback part easy and consequently more robust.

The current approach with the lookahead concept is working well, but there are rooms to investigate this concept more.

Tracking vehicle position to use as main input for the controllers seems infeasible due to slow update rate of such data in a real collision avoidance application. However, such data can be used with a slower rate in parallel to help the vehicle correct its trajectory. In addition to what is already investigated in this work, another approach in this regard would be refreshing path planning on a certain rate of occurrence during the manoeuvre based on newly received information from the position of the vehicle.

The simulation tool developed in this work, provides the possibility to integrate steering and braking in future works. Although a brief investigation is done as presented in [27], it remains as one of the main works for the future. In this regard, adding an ABS brake model and rotating wheels can also help the simulation to be more realistic in presence of the brake actuators.

Rear-wheel steering can be used to improve the manoeuvrability of the vehicle. It would also be advantageous, because it can reduce the required front wheel steering angle and consequently will decrease the requirements on the steering actuator. This is also favourable when the interaction with driver is considered.

Appendix A Tyre modelling and relevant assumptions

Tyre behaviour is nonlinear and dependent on several parameters like tyre structure, road condition, and load distribution. The nonlinearity increases significantly in an emergency manoeuvre when tyre force saturation can also take a highly limiting action. In order to capture the nonlinearity in a tyre model as much as possible, and without getting into extensive real tyre data exploration, some approximations need to be made to include the most important materials, *i.e.* adhesion coefficient, cornering stiffness, and Magic Tyre Formula. As a result, it would be possible to calculate tyre forces and to better understand the response of the tyres in different dynamical states of the vehicle.

A.1 Adhesion coefficient and its alteration with the vertical load

Adhesion coefficient is shown to be nonlinearly decreasing with vertical load [28]. In order to simplify this relation, it is approximated as a linear relation as

$$\mu = -\mu_1 F_z + \mu_2, \tag{A.1}$$

where μ and F_z are adhesion coefficient and vertical load on a wheel, respectively. μ_1 and μ_2 are coefficients that need to be derived so that they satisfy two conditions. First, Equation A.1 should result in peak value of adhesion coefficient, μ_p, for laden static load. Second, in the case of extreme load transfer, *i.e.* when one side of the axle is lifted up, it should result in reduced value of the adhesion coefficient, μ_d. Therefore μ_1 and μ_2 can be calculated as

$$\begin{aligned} \mu_1 &= \frac{\mu_p - \mu_r}{F_{z0}}, \\ \mu_2 &= 2\mu_p - \mu_r, \end{aligned} \tag{A.2}$$

where F_{z0} is static load on the wheel, and μ_p and μ_r are constants that are dependent on the road and operating condition, and may be found in parameter settings for simulation.

A.2 Cornering stiffness and its alteration with the vertical load

The cornering stiffness, $\left(\frac{\partial F_y}{\partial \alpha}\right)_{\alpha=0}$, increases degressively with vertical load for a pneumatic tyre. Its nonlinearity may be approximated by a quadratic function as

$$C_\alpha = C_1 {F_z}^2 + C_2 F_z, \tag{A.3}$$

where C_1 and C_2 are coefficients that are calculated based on available values for known conditions of the vehicle, and may be found among vehicle data in Table of notations in appendices.

A.3 The Magic Tyre Formula parameters

The Magic Tyre Formula [24] is a very useful tool to model tyre forces with respect to the slip angles. It provides a *magically* good fit to the experimental tyre data, thus making it attractive to use in vehicle dynamics simulations. Pure lateral slip condition is described first here, and then it is used to calculate lateral force given the longitudinal force as an input in combined slip condition and also in the presence of vertical load transfer.

The lateral force in pure lateral slip condition is denoted by F_{y0} and can be expressed as below, assuming zero camber, conicity, and ply-steer:

$$F_{y0} = D \sin\big(C \arctan\big(B\alpha - E(B\alpha - \arctan(B\alpha))\big)\big). \tag{A.4}$$

Parameters B, C, D, and E define the Magic Formula, and can be determined using regression techniques, provided the experimental tyre data was available for variation of tyre forces versus slip angle. Here, all these parameters are borrowed from [24] as follows.

The peak value of side force, D, can simply be calculated as

$$D = \mu F_z. \quad \text{A.5}$$

The shape factor, C, can be calculated as

$$C = 1 \pm \left(1 - \frac{2}{\pi}\arcsin\left(\frac{F_{y,a}}{D}\right)\right), \quad \text{A.6}$$

where $F_{y,a}$ represents the value for horizontal asymptote of the lateral force variations versus slip angle. The ratio $F_{y,a}$ / D can be approximated with the ratio of μ_s /μ_p where μ_p and μ_s are peak and sliding values of the road adhesion coefficient. Their value may be measured through experiments, or be assumed based on published data, *e.g.* in Table 1.3 of [29], as is done in this work and may be found in parameter settings for simulation.

As for the curvature factor, E, one can write:

$$E = \frac{B\alpha_m - \tan\left(\frac{\pi}{2C}\right)}{B\alpha_m - \arctan(B\alpha_m)}, \quad \text{A.7}$$

where α_m is the slip angle corresponding to the maximum lateral force. It varies directly with the vertical load, so that the point where tyre force reaches to its peak, laterally shifts in the diagram of tyre force versus slip angle. This dependency on vertical load is approximated as a linear variation that covers two extreme cases; in the vicinity of zero vertical load and in the case of extreme load transfer when the inner wheel is lifted up. For the first case the peak value occurs at α_r, and it occurs at α_p for the other one. Then the value for α_m can be calculated as

$$\alpha_m = \left(\alpha_r + \left(\frac{\alpha_p - \alpha_r}{2}\right)\frac{F_{z,n}}{F_{z0,n}}\right)\frac{\pi}{180}, \quad \text{A.8}$$

where α_r and α_p may be found in parameter settings for simulation.

Finally, the stiffness factor, B, can now be calculated as below:

$$B = \frac{BCD}{CD} = \frac{C_\alpha}{CD}. \quad \text{A.9}$$

By introduction of any longitudinal force, *e.g.* braking while cornering, the tyre will enter into the combined slip condition and the maximum lateral force that it can generate will decrease. In addition, the tyre stiffness and slip angle will also be influenced.

The stiffness in new condition can be calculated as

$$C_{F\alpha} = \phi_{x\alpha}\left(C_\alpha - \frac{1}{2}\mu F_z\right) + \frac{1}{2}(\mu F_z - F_x), \quad \text{A.10}$$

with

$$\phi_{x\alpha} = \left(1 - \left(\frac{F_x}{\mu F_z}\right)^n\right)^{\frac{1}{n}}, \quad \text{A.11}$$

where n can vary between 2 and 8.

The equivalent slip angle can be calculated as

$$\alpha_{eq} = \frac{1}{\phi_x}\frac{C_{F\alpha}}{C_\alpha}\frac{\mu_0 F_{z0}}{\mu F_z}\alpha, \quad \text{A.12}$$

where F_{z0} represents nominal load on wheel, and associated friction coefficient is represented by μ_0. ϕ_x is a factor that can be calculated as

$$\phi_x = \frac{\sqrt{(\mu F_z)^2 - F_x^2}}{\mu F_z}. \quad \text{A.13}$$

Finally, the lateral force on tyre can be calculated as

$$F_y = \phi_x \frac{\mu F_z}{\mu_0 F_{z0}} F_{y0}, \qquad \text{A.14}$$

where F_{y0} can be calculated using Equation but employing the equivalent slip angle from Equation A.11.

Similar to lateral force, the longitudinal force also has to be limited. On the one hand, when the wheel is locked due to intense braking, the whole wheel starts to slide and the force generation is altered. The wheel then acts like a solid object exposed to Coulomb friction, and sliding on the road surface. This means that the resulted tyre force is parallel but in opposite direction to the sliding velocity vector at the tyre contact patch. On the other hand, in the case of excessive traction torque applied on the wheel, the force generation is not altered because a wheel on which a traction torque is applied cannot behave like a locked wheel, *i.e.* absolute value of the longitudinal slip never reaches 100% unless the vehicle is fixed. Therefore, the following interval can be written for the longitudinal tyre force:

$$-\mu F_z \cos\alpha \le F_x \le \mu F_z. \qquad \text{A.15}$$

An important point to be considered here is the dependence of the adhesion coefficient on the slip angle. This dependency would highly affect the adhesion coefficient in presence of big slip angles. Once the peak point in the tyre lateral force *vs.* slip angle characteristic curve is exceeded, the whole tread starts to slide. Then, the adhesion coefficient decreases with the slip angle. More explanations can be found in [30] where Stribeck effect is introduced. When full sliding starts, the available adhesion coefficient, in the case of zero longitudinal force, will be corrected as below:

$$\mu = \frac{|F_y|}{F_z} \ , \ if \ |\alpha| > \alpha_m. \qquad \text{A.16}$$

Tyre characteristics can be reviewed in following figures for parameter values given in Table of notations. Variation of normalized lateral force versus slip angle is plotted in Figure A.1, for a few different loading ratios, but for longitudinal force set to zero. Dotted curves are derived from pure slip model as can be calculated using Equation A.3, whereas the continues curves represent simplified combined slip model that takes both load transfer and longitudinal force into account in a more proper way.

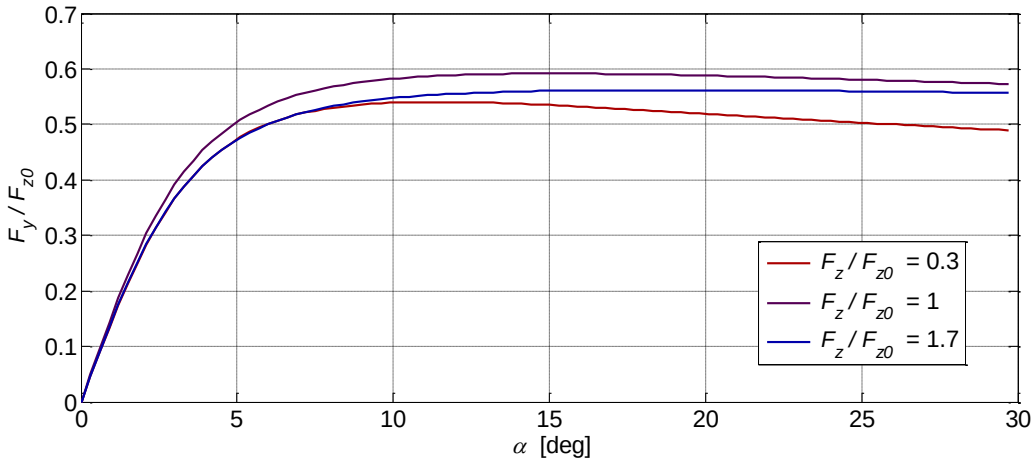

Figure A.1 Normalized lateral force vs. slip angle for different vertical load ratios and zero longitudinal force.

Although the longitudinal force is zero for both set of curves, there are significant differences between two models in presence of the vertical load transfer.

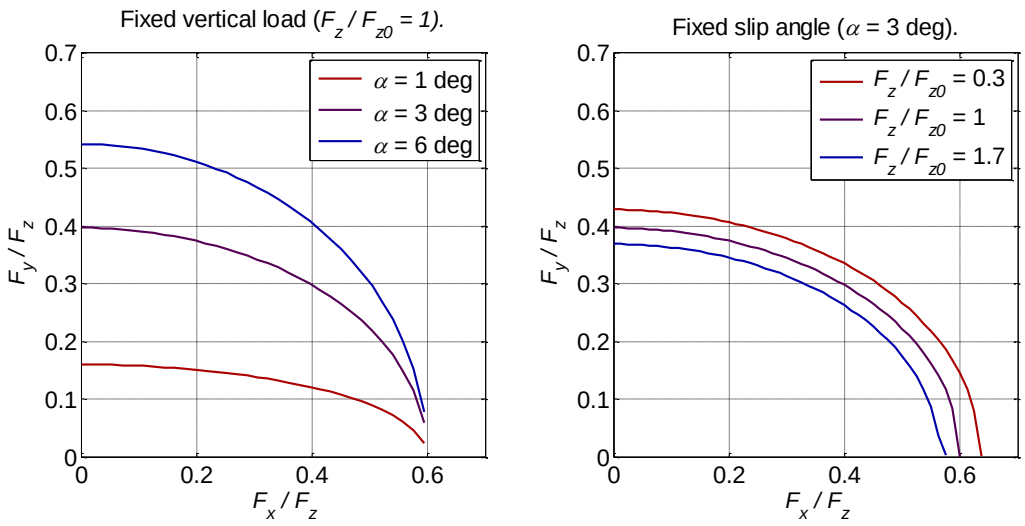

Figure A.2 Variation of normalized lateral vs. longitudinal force, for different loading condition and slip angles.

Appendix B Fifth order polynomial

Considering a fifth order polynomial as

$$y = \sum_{i=1}^{6} c_i x^{i-1} = c_1 + c_2 x + c_3 x^2 + c_4 x^3 + c_5 x^4 + c_6 x^5$$

where x and y are longitudinal and lateral position, and c_i represents coefficients of the fifth order polynomial. The function "polynomial5" performs necessary calculations to determine coefficients. It takes in a range for "x" as called "xBoundary", a number of points ("x") in the range, which corresponding polynomial data is asked for, initial and final boundary conditions for y ("iBCND" and "fBCND" respectively) which include y, y', and y'', and returns vectors for fifth order polynomial y, and its first and second derivatives with respect to x. Calculating the first and second derivatives of the equation above, gives:

$$y' = \sum_{i=2}^{6} c_i (i-1) x^{i-2} = c_2 + 2c_3 x + 3c_4 x^2 + 4c_5 x^3 + 5c_6 x^4$$

$$y'' = \sum_{i=3}^{6} c_i (i-1)(i-2) x^{i-3} = 2c_3 + 6c_4 x + 12c_5 x^2 + 20c_6 x^3$$

Now using these three equations and given boundary conditions, the corresponding fifth order polynomial can be determined.

```
function [y, yPrime, yDPrime] = polynomial5(x, xBoundary, iBCND, fBCND)
c = zeros(1, 6);
```

This function is calculating a fifth order polynomial, which connects start point to the final point. The result can be translated in one direction, e.g. x-direction, provided the corresponding boundary conditions are also translated. So, if one moves the resulting curve in the horizontal direction values of "y" will not change. Thus, for the ease of calculations, all points are moved horizontally to put the start of the "xRange" on the origin of the coordinate system.

```
xLocal = x - xBoundary(1);
```

Boundary conditions can be found in the inputs to the function and are required to calculate multipliers by inserting them into the first 3 equations above:

```
x1      = xBoundary(1);
x2      = xBoundary(2);
y1      = iBCND(1);
yPrime1 = iBCND(2);
yDPrime1 = iBCND(3);
y2      = fBCND(1);
yPrime2 = fBCND(2);
yDPrime2 = fBCND(3);
```

$$x_1 = 0 \Rightarrow \begin{cases} c_1 = y_1 \\ c_2 = y_1' \\ c_3 = \frac{1}{2} y_1'' \end{cases}$$

```
c(1) = y1;
c(2) = yPrime1;
c(3) = 0.5 * yDPrime1;
```

Using other initial conditions and solving resulting equations for other multipliers, other remaining multipliers can be calculated:

$$c_4 = 10\frac{y_2 - y_1}{(x_2 - x_1)^3} - \frac{6y_1' + 4y_2'}{(x_2 - x_1)^2} - \frac{3y_1'' - y_2''}{2(x_2 - x_1)}$$

```
c(4) = 10 * (y2 - y1) / (x2 - x1) ^ 3 ...
    - (6 * yPrime1 + 4 * yPrime2) / (x2 - x1) ^ 2 ...
    - (3 * yDPrime1 - yDPrime2) / (2 * (x2 - x1));
```

$$c_5 = 15\frac{y_1 - y_2}{(x_2 - x_1)^4} + \frac{8y_1' + 7y_2'}{(x_2 - x_1)^3} + \frac{\frac{3}{2}y_1'' - y_2''}{(x_2 - x_1)^2}$$

```
c(5) = 15 * (y1 - y2) / (x2 - x1) ^ 4 ...
    + (8 * yPrime1 + 7 * yPrime2) / (x2 - x1) ^ 3 ...
    + (1.5 * yDPrime1 - yDPrime2) / (x2 - x1) ^ 2;
```

$$c_6 = 6\frac{y_2 - y_1}{(x_2 - x_1)^5} - 3\frac{y_1' + y_2'}{(x_2 - x_1)^4} - \frac{y_1'' - y_2''}{2(x_2 - x_1)^3}$$

```
c(6) = 6 * (y2 - y1) / (x2 - x1) ^ 5 ...
    - 3 * (yPrime1 + yPrime2) / (x2 - x1) ^ 4 ...
    - 0.5 * (yDPrime1 - yDPrime2) / (x2 - x1) ^ 3;
```

Now recalling the first 3 equations as below, and having multipliers one can easily calculate y, y', and y''.

$$y = \sum_{i=1}^{6} c_i x^{i-1}$$

$$y' = \sum_{i=2}^{6} c_i (i-1) x^{i-2}$$

$$y'' = \sum_{i=3}^{6} c_i (i-1)(i-2) x^{i-3}$$

```
nPoints = length(x);
y     = zeros(1, nPoints);
yPrime  = zeros(1, nPoints);
yDPrime = zeros(1, nPoints);
for i = 1:6
    y  = y + c(i) * xLocal .^ (i - 1);
    if (i >= 2)
        yPrime  = yPrime  + c(i) * (i - 1) * xLocal .^ (i - 2);
    end
    if(i >= 3)
        yDPrime = yDPrime + c(i) * (i - 1) * (i - 2) * xLocal .^ (i - 3);
    end
end
end
```

Literature

1. *Accident avoidance by active intervention for Intelligent Vehicles (interactIVe)*. 2010-13; Integrated Project co-funded by the European Commission]. Available from: http://www.interactive-ip.eu.
2. Seiniger, P., et al., *Deliverable D7.3 | Legal Aspects*, 2012, EU Project interactIVe.
3. Mäkinen, T., et al., *Deliverable D1.5 | Use cases and requirements*, 2010, EU Project interactIVe.
4. Lytrivis, P., et al., *Deliverable D2.1 | Perception requirements on sensor interfaces, sensor data fusion, and perception horizon interface*, 2010, EU Project interactIVe.
5. Vahidi, A. and A. Eskandarian, *Research advances in intelligent collision avoidance and adaptive cruise control.* Intelligent Transportation Systems, IEEE Transactions on, 2003. **4**(3): p. 143-153.
6. Araki, H., et al. *Development of rear-end collision avoidance system*. in *Intelligent Vehicles Symposium, 1996., Proceedings of the 1996 IEEE*. 1996.
7. Broxmeyer, C., *Vehicle longitudinal control and collision avoidance system for an automated highway system*, U.S. Patent, Editor 1994.
8. Shaw, D.C.H. and J.Z.Z. Shaw, *Vehicle collision avoidance system*, U.S. Patent, Editor 1996: United States.
9. Gerdes, J.C. and E.J. Rossetter, *A Unified Approach to Driver Assistance Systems Based on Artificial Potential Fields.* Journal of Dynamic Systems, Measurement, and Control, 2001. **123**(3): p. 431-438.
10. Resende, P. and F. Nashashibi. *Real-time dynamic trajectory planning for highly automated driving in highways*. in *Intelligent Transportation Systems (ITSC), 2010 13th International IEEE Conference on*.
11. Petrov, P. and F. Nashashibi. *Planning and nonlinear adaptive control for an automated overtaking maneuver*. in *Intelligent Transportation Systems (ITSC), 2011 14th International IEEE Conference on*.
12. Hiraoka, T., O. Nishihara, and H. Kumamoto, *Automatic path-tracking controller of a four-wheel steering vehicle.* Vehicle System Dynamics: International Journal of Vehicle Mechanics and Mobility, 2009. **47**(10): p. 1205-1227.
13. Thommyppillai, M., S. Evangelou, and R.S. Sharp, *Car driving at the limit by adaptive linear optimal preview control.* Vehicle System Dynamics: International Journal of Vehicle Mechanics and Mobility, 2009. **47**(12): p. 1535-1550.
14. Kritayakirana, K. and J.C. Gerdes. *Autonomous Cornering at the Limits: Designing a Longitudinal Feedback Controller Using a Tire Slip Circle*. in *Proceedings of the 10th international symposium on advanced vehicle control*.
15. Kritayakirana, K. and J.C. Gerdes, *Using the center of percussion to generate feedforward steering for an autonomous race car*, in *22nd International Association for Vehicle System Dynamics (IAVSD) Symposium on Dynamics of Vehicles on Roads and Tracks*2011: Manchester, United Kingdom.
16. Kritayakirana, K. and J.C. Gerdes, *Using the centre of percussion to design a steering controller for an autonomous race car.* Vehicle System Dynamics, 2012. **50**(sup1): p. 33-51.
17. Nozad, A., et al. *Optimal path recovery from terminal understeer*. in *Proceedings of 22nd IAVSD Symposium on Dynamics of Vehicles on Roads and Tracks*.
18. Rutquist, P.E. and M.M. Edvall, *PROPT - Matlab Optimal Control Software*, 2010.
19. Bilen, Ö.B., *Path Control Algorithms for Autonomous Steering and Braking of Heavy Vehicles*, 2010, Chalmers University of Technology.
20. Heisler, H., *Advanced vehicle technology*. 2002: Butterworth-Heinemann.

21. Matschinsky, W. and A. Baker, *Road vehicle suspensions*. 2000: Professional Engineering Pub.
22. Volvo, T.C., *Volvo Truck FH 62R B3LH1 Data Sheet*, 2009.
23. Milliken, W.F. and D.L. Milliken, *Race car vehicle dynamics*. 1995: Society of Automotive Engineers.
24. Pacejka, H.B., *Tyre and vehicle dynamics*. 2006: Butterworth-Heinemann.
25. Maurice, J.P. and H.B. Pacejka, *Relaxation Length Behaviour of Tyres.* Vehicle System Dynamics, 1997. **27**(sup001): p. 339-342.
26. Williams, D.E., *On the equivalent wheelbase of a three-axle vehicle.* Vehicle System Dynamics, 2011. **49**(9): p. 1521-1532.
27. Hassanzadeh, M., et al. *Path and speed control of a heavy vehicle for collision avoidance manoeuvres*. in *Intelligent Vehicles Symposium (IV), 2012 IEEE*. 2012.
28. Segel, L. and R.D. Ervin, *The Influence of Tire Factors on the Stability of Trucks and Tractor Trailers.* Vehicle System Dynamics: International Journal of Vehicle Mechanics and Mobility, 1981. **10**(1): p. 39-59.
29. Wong, J.Y., *Theory of ground vehicles*. 2001: John Wiley.
30. Liang, W., J. Medanic, and R. Ruhl, *Analytical dynamic tire model.* Vehicle System Dynamics: International Journal of Vehicle Mechanics and Mobility, 2008. **46**(3): p. 197-227.

Table of notations

Notation	Value	Unit	Description
B	–	$\mathrm{N/rad}$	Stiffness factor in Magic Tyre Formula
C	–	–	Shape factor in Magic Tyre Formula
$C_{1,n}$	-2×10^{-5}	$1/\mathrm{N}^2$	First coefficient in calculation of cornering stiffness
$C_{2,n}\big\vert_{n=1,2}$	5.8614	$1/\mathrm{N}$	Second coefficient in calculation of cornering stiffness
$C_{2,n}\big\vert_{n=3,\ldots,6}$	6.515	$1/\mathrm{N}$	Second coefficient in calculation of cornering stiffness
C_ϕ	86000	$\mathrm{Nms/rad}$	Roll damping
$C_{\phi,1}$	28000	$\mathrm{Nms/rad}$	Roll damping of first axle
$C_{\phi,2}$	29000	$\mathrm{Nms/rad}$	Roll damping of second axle
$C_{\phi,3}$	29000	$\mathrm{Nms/rad}$	Roll damping of third axle
D	–	N	Peak value in Magic Tyre Formula
E	–	–	Curvature factor in Magic Tyre Formula
$F_{x,n}$	–	N	Longitudinal force on n^{th} wheel
$F_{y,n}$	–	N	Lateral force on n^{th} wheel
F_{dyn}	–	N	The force corresponding to the dynamical condition
$F_{z,i,stat}$	–	N	Static load on i^{th} axle
$F_{z,n,stat}$	–	N	Static load on n^{th} wheel
I_{xx}	19000	$\mathrm{Kgm2}$	Vehicle moment of inertia around x axis
$I_{xx,s}$	–	Kgm^2	Sprung mass moment of inertia around x axis
I_{zz}	150000	Kgm^2	Vehicle moment of inertia around z axis
K_{PY}	–	$\mathrm{rad/m}$	Controller gain, lateral position control
K_{IY}	–	$\mathrm{rad/\,m.s}$	Controller gain, lateral position control
K_{DY}	–	$\mathrm{s.rad/m}$	Controller gain, lateral position control
$K_{P\psi}$	–	–	Controller gain, yaw control
$K_{D\psi}$	–	s	Controller gain, yaw control
K_{PV}	–	$\mathrm{kg/s}$	Controller gain, speed control
K_{PS}	–	$\mathrm{kgm/s.rad}$	Controller gain, direct yaw moment control

Notation	Value	Unit	Description
K_ϕ	1.54×10^6	$\mathrm{Nm/rad}$	Roll stiffness
$K_{\phi,1}$	380000	$\mathrm{Nm/rad}$	Roll stiffness of first axle
$K_{\phi,2}$	580000	$\mathrm{Nm/rad}$	Roll stiffness of second axle
$K_{\phi,3}$	580000	$\mathrm{Nm/rad}$	Roll stiffness of third axle
$K_{\phi,2+3}$	–	$\mathrm{Nm/rad}$	Roll stiffness of tandem axle
L	4.900	m	Distance between the first and the second axle
L_1	3.976	m	Distance between CG and the first axle
L_2	0.924	m	Distance between CG and the second axle ($L - L_1$)
L_3	2.294	m	Distance between CG and the third axle ($L + L_{bs} - L_1$)
L_{bs}	1.370	m	Total length of the truck
L_e	–	m	Equivalent wheel base;
L_fo	1.360	m	Front overhang
L_max	10.305	m	Total length of the truck
L_ro	2.675	m	Rear overhang ($L\_max - L - L\_bs - L\_fo$)
L_t	5.441	m	Theoretical wheel base
M_z	–	Nm	Vehicle yaw moment
W	2.050	m	Track width of the truck
W_max	2.495	m	Total width of the truck
X	–	m	Longitudinal position in global coordinate system
X_is	–	m	Longitudinal position of the intervention start point
Y	–	m	Lateral position in global coordinate system
a_x	–	$\mathrm{m/s^2}$	Longitudinal acceleration
a_y	–	$\mathrm{m/s^2}$	Lateral acceleration
b	–	m	Lateral displacement
b_max	–	m	Maximum feasible lateral displacement
c_δ	4.88×10^{-7}	$\mathrm{rad/N}$	Steering compliance
d	–	m	Longitudinal distance of the reference path.
d_c	–	m	Longitudinal distance of critical path
d_la	–	m	Lookahead distance
g	9.81	$\mathrm{m/s^2}$	Gravitational acceleration
h	–	m	Height of centre of gravity (CG) from ground
h_1	0.3	m	Roll centre height of first axle
h_2	0.8	m	Roll centre height of second axle
h_3	0.8	m	Roll centre height of third axle
h'	0.9	m	Height of centre of gravity (CG) from roll centre (RC)
i	1,2,3	–	Index number of axles starting from front to rear

Notation	Value	Unit	Description
i_s	20	–	Steering gear ratio
l_n	–	m	Longitudinal position of n^{th} wheel in the coordinate system fixed to the vehicle
m	26500	kg	Vehicle mass
m_s	24000	kg	Sprung mass
m_u	2500	kg	Unsprung mass
n	$1,2,\ldots,6$	–	Index number of wheels starting from front and left (1) to rear and right (6)
t_{la}	–	s	Lookahead time
v_x	–	m/s	Longitudinal speed of the vehicle
v_y	–	m/s	Lateral speed of the vehicle
w_n	–	m	Lateral position of n^{th} wheel in the coordinate system fixed to the vehicle
$\Delta F_{z,i}$	–	N	Load transfer on i^{th} axle
α	–	rad	Slip angle
α_m	–	rad	Slip angle for which maximum lateral force is generated
δ	–	rad	Steering angle
δ_n	–	rad	Wheel angle of n^{th} wheel
ε_1	0.14	–	Roll steer coefficient of front left wheel
ε_2	0.14	–	Roll steer coefficient of front right wheel
ε_3	-0.10	–	Roll steer coefficient of dual wheels on the left
ε_4	-0.10	–	Roll steer coefficient of dual wheels on the right
ε_5	-0.10	–	Roll steer coefficient of rear left wheel
ε_6	-0.10	–	Roll steer coefficient of rear right wheel
ζ	–	%	Safety margin for a manoeuvre
η	–	–	Manoeuvre severity
μ_1	–	1/N	The first coefficient in adhesion calculations
μ_2	0.65	–	The second coefficient in adhesion calculations
σ_x	0.4	m	Longitudinal relaxation length
σ_y	0.2	m	Lateral relaxation length
ϕ	–	rad	Roll angle
ψ	–	rad	Yaw angle